Complex Engineering Systems

Research Article

H$_\infty$ fault-tolerant decentralized observer-based PID team formation tracking design for NCS of large-scale LEO satellites

Bor-Sen Chen, Chuan-Cheng Liang, Lu-Heng Wang

Department of Electrical Engineering, National Tsing Hua University, Hsinchu 30013, Taiwan.

Correspondence to: Prof. Bor-Sen Chen, Department of Electrical Engineering, National Tsing Hua University, No. 101, Section 2, Kuang-Fu Road, Hsinchu 30013, Taiwan. E-mail: bschen@ee.nthu.edu.tw

Abstract

In this study, a simple decentralized H$_\infty$ fault-tolerant observer-based proportional-integral-derivative formation tracking design is proposed for network control systems of large-scale low earth orbit satellites under external disturbance, coupling and malicious attack signals via wireless communication channels. First, a novel reference-based feedforward linearization control scheme is introduced, transforming the nonlinear formation output feedback tracking control problem into an equivalent linearized formation tracking control system of each satellite. To prevent faults from corrupting the estimation and control of the satellite formation, two novel smoothing models of actuator and sensor fault signals are embedded in the equivalent linearized formation system of each satellite. Then, a decentralized H$_\infty$ fault-tolerant observer-based proportional-integral-derivative control strategy is proposed to efficiently attenuate the effect of actuator and sensor faults, measurement noise and satellite coupling on the overall team formation. We only need to solve a linear matrix inequality-constrained optimization problem for each satellite to achieve the optimal H$_\infty$ formation problem. Finally, a team formation example with twelve satellites crossing four orbits for a specific mission is provided to validate the proposed design, comparing it with other methods.

Keywords: H$_\infty$, network control system, LEO, team formation control, fault-tolerant control, PID control, observer, smoothing model

1. INTRODUCTION

Recently, due to the anticipated future development of 5G and 6G in wireless communication networks, low earth orbit (LEO) satellites have gained attention for their low power consumption and minimal transmission delay, making them a very popular topic in various research areas[1,2]. In the Amazon, Telesat and SpaceX's project[3], based on the above advantages in systematic characteristics, a very large amount of LEO satellites have been employed for developing a team formation of large-scale satellites or satellite constellations. In the future, large-scale team formations of satellites can enable LEO satellites to attain the global coverage of the earth and solve the corresponding service of satellite coverage for global wireless communication networks in the 5G and 6G era.

Further, LEO satellites need to establish communication with other satellites through Laser Inter Satellite Links (LISLs)[4]. Therefore, their communication is not retrieved to the ground station, but to achieve a more efficient transmission in satellite communication. However, in order to attain an ideal large-scale team formation for ideal service coverage, the altitude and attitude of large-scale LEO satellites must be efficiently estimated and precisely controlled in the ground station based on the desired mission during their flying processes. Therefore, the team formation observer-based trajectory estimation and reference tracking control of large-scale LEO satellites will become an important research topic.

As for the team formation control methods, the leader-follower (L-F) method is the most common due to its relatively simple implementation[5,6]. Followers can be controlled to achieve a desired team formation shape with the leader by keeping at specific altitudes and attitudes. However, in the L-F method, if the leader crashes due to an accident, the formation cannot be maintained[7]. Therefore, the virtual-leader (V-L) scheme is increasingly considered the most suitable team formation control method for practical applications, as it does not crash under a disturbed environment[8,9].

Except for the above methods, team formation tracking control schemes are also suitable for large-scale team formation control systems. In general, they can be separated into centralized[10,11] and decentralized team formation tracking control strategies[12,13]. In the centralized team formation tracking control strategy of satellites, all satellites need to be integrated as a very large augmented system and coordinated by a single large controller. Therefore, this may significantly increase the design difficulty and control computational complexity because the team formation of all satellites has to be achieved simultaneously by one controller and the information of all satellites needs to be processed at once. In general, it is very difficult to design a centralized team formation tracking control for multiple quadrotor unmanned aerial vehicles (UAVs). However, the decentralized team formation control strategy of large-scale satellites can be designed independently for each satellite[14,15]. Therefore, the decentralized strategy is more suitable for the team formation control design of large-scale LEO satellites in this study.

In the future 5G and 6G era, to meet the development and application of wireless communication networks, the network control technologies of multi-agents have been widely applied in various research areas[16]. Therefore, in this paper, network control system (NCS) technologies are applied to team formation control design for large-scale LEO satellites, i.e., transmitting the trajectory and control information of each LEO satellite via wireless communication networks. In this situation, the trajectory information of LEO satellites is transmitted from a sender to a ground control station (GCS). Then, GCS estimates the trajectory information by a Luenberger observer from the measured signal and calculates the control signal back for each LEO satellite achieving the desired satellite team formation for a coverage mission[17]. However, the transmission information of output measurement of satellites to the receiver of GCS and control commands from its sender to actuators of satellites via wireless network will suffer from measurement noise, channel noise and malicious attack signals, resulting in the degradation of trajectory estimation and formation tracking performance of NCS of large-scale LEO satellites. In the conventional proportional-integral-derivative (PID) control designs, they always lie in the local linearized systems. Further, PID control designs are seldom applied to large-scale nonlinear dynamic systems with external disturbances, measurement noise, attack signals, and couplings. Therefore, a decentralized observer-based PID control design is appealing for the robust team formation tracking control design of large-scale NCS of LEO satellites in the future. To overcome the effect of malicious attack signals on the degradation of trajectory estimation performance of satellites by a Luenberger observer and on the degradation of PID team formation tracking control performance of LEO satellites, a decentralized robust H_∞ observer-based fault-tolerant PID team formation control strategy is proposed to efficiently eliminate the effect of malicious attack signals on the trajectory estimation performance of Luenberger observers and team formation tracking performance of PID controllers of NCS of large-scale LEO satellites. Recently, fault-tolerant control (FTC) schemes have been a popular research topic and aimed at estimating

these attack signals for compensating control of these attack signals [18,19]. In this study, a smoothing signal model based on the extrapolation method is employed without updating model parameters to efficiently estimate attack signals for compensation control to avoid their effect on trajectory estimation and control performance. With these two smoothing signal models being embedded in the dynamic model of the LEO satellite, the two attack signals on the actuator and sensor of LEO satellites can be efficiently estimated and their corruption on team formation can be effectually eliminated by the proposed robust decentralized H_∞ fault-tolerant observer-based PID team formation control strategy for the NCS of LEO satellites.

To achieve global coverage for LEO satellite services in the 6G era, the number of LEO satellites in NCS needs to be significantly increased. Therefore, the coupling effects among satellites are unavoidable in the wireless communication network, i.e., co-channel interference (CCI), and must be considered in the observer-based team formation traveling control design of NCS of large-scale LEO satellites [20]. Furthermore, sensor measurement noise and external disturbances affecting satellites are inevitable in the trajectory estimation and formation control of satellites. External disturbances in outer space include the Earth's flattening, aerodynamic drag, solar radiation pressure, and others [21–23]. Consequently, the H_∞ fault-tolerant decentralized robust observer-based team formation control strategy is essential for the NCS of large-scale satellites [24,25] to efficiently estimate the attack signals for compensation, eliminate the effect of external disturbances, measurement noise and coupling from other satellites, and achieve the desired team formation for coverage tasks of large-scale LEO satellite NCS. However, since the system dynamic model of relative positions and attitudes of large-scale satellite systems is very complicated and highly nonlinear, it is necessary to solve a corresponding highly nonlinear partial differential Hamilton Jacobi Isaac equation (HJIE) for robust decentralized H_∞ fault-tolerant observer-based team formation control design of each satellite [24,25].

At present, it is still very difficult to efficiently solve this HJIE analytically or numerically. Previously, the altitude and attitude control of satellites have always been designed separately [26]. Recently, to deal with this difficult HJIE problem, the fuzzy interpolation method has been employed for interpolating several local linearized satellite systems at some desired operation points to efficiently approximate the highly nonlinear satellite dynamic system so that the HJIE of each satellite can be transformed to a set of Riccati-like equations and then a set of easier solvable linear matrix inequalities (LMIs) [24,27]. Nevertheless, the transformation process from HJIE to a set of LMIs needs to perform a series of inequality operations, leading to very conservative results. Furthermore, the observer-based team formation fuzzy control requires very complex calculations for each satellite to obtain observer-based fuzzy team formation control signals. More recently, a HJIE-reinforcement deep learning algorithm has been employed to train deep neural networks (DNN) to solve HJIE for the robust H_∞ observer-based fault-tolerant decentralized formation control of NCS of large-scale LEO satellites [25]. However, the design procedure is divided into off-line training and online operation phases, separately, and the implementation of decentralized H_∞ HJIE-reinforcement DNN-based observer-based fault-tolerant team formation tracking control of LEO satellites seems still complicated and more effort is still needed for practice application.

The conventional PID control has been successfully applied to control designs of linear satellites with several practical applications due to their simple structure and easy implementation with adequate performance [28–33]. Recently, an adaptive PID controller has been proposed for FTC of a quadrotor helicopter system [34]. Robust PID control has been proposed in [31]. A nonlinear PID control has been employed for a quadrotor UAV [32]. However, traditional PID control designs are always based on a local linearized mode at an operation point of a nonlinear dynamic system. Since a nonlinear system such as a satellite has many operation points, a set of PID controllers are typically required to operate at different operation points. Recently, approaches involving the fuzzy interpolation of local linearized systems have been explored to approximate nonlinear systems such as quadrotor UAVs. For example, PID controllers can be interpolated through fuzzy bases to achieve decentralized fuzzy reference tracking control for large-scale quadrotor UAVs. However, if only output measurements are used and a fuzzy observer-based PID controller is employed, the number of required local fuzzy observer-based PID controllers can grow significantly, making the design overly complex. This complexity, combined with challenges such as external disturbances, measurement noise, and system coupling, has hindered the development of observer-based PID control designs for highly nonlinear systems such as quadrotor UAVs and satellites.

Therefore, in this study, a novel reference-based feedforward linearization observer-based PID team formation design is proposed to achieve a decentralized robust H_∞ fault-tolerant observer-based team formation tracking control of NCS of large-scale LEO satellites under measurement noise, external disturbances and couplings. First, a reference-based feedforward linearization tracking control is proposed for each satellite to achieve a linear team formation tracking

error system with an equivalent actuator false signal including the error of reference-based feedforward linearization, actuator attack signal, and coupling from other satellites, and an output measurement system with sensor false signals including sensor attack signal and measurement noise. Then, a smoothing signal model is employed to describe the actuator and sensor false signal. Furthermore, two smoothing signal models of equivalent actuator and sensor fault signals are embedded in the decoupled augmented linear formation tracking system in (17) of each LEO satellite to avoid the corruption of the estimation and formation tracking control due to actuator and sensor faults. The actuator and sensor fault signals can be estimated by conventional Luenberger observers for compensating their corruption effect on the team formation tracking control process. Then, an observer-based PID control design in (19) is proposed to achieve the robust decentralized H_∞ fault-tolerant estimation and team formation tracking control strategy in (22) of each LEO satellite. This can be reformulated as a two-LMI-constrained problem, solvable through a two-step design procedure for each satellite in team formation. In this situation, using the LMI Toolbox in MATLAB, we can obtain the observer gain and control parameters for the observer-based PID controller easily to satisfy a two LMIs-constrained problem, enabling the robust H_∞ decentralized fault-tolerant observer-based PID team formation design of NCS of large-scale LEO satellites with a prescribed disturbance attenuation level ρ. To avoid the integration of the PID controller, an actuator saturation constraint is also considered with an equivalent LMI constraint in the design procedure. Therefore, if the optimal H_∞ fault-tolerant decentralized observer-based PID team formation control strategy is considered with an actuator saturation constraint, then we only need to solve a three-LMI-constrained optimization problem, which can be solved by decreasing ρ until no solution of positive definite matrix $P^T = P > 0$ of the quadratic Lyapunov function exists. Therefore, the corresponding PID control parameters $\bar{k}_i$ and observer gain L_i, as given in (19), can be obtained in a single run using the LMI Toolbox via MATLAB, thus avoiding the complex parametric tuning process of the conventional PID controller design. This approach achieves the optimal robust H_∞ fault-tolerant decentralized observer-based PID team formation design of the NCS of large-scale LEO satellites.

In the future 5G and 6G wireless communication network era, a large-scale constellation of LEO satellites will be developed for global service coverage of the Earth. In this situation, the crossing among these satellite orbits is unavoidable in the limited space. Therefore, the team formation of large-scale LEO satellites of different satellite orbits is necessary for the future satellite constellation era. At the end of this study, a simulation example of a team formation of 12 LEO satellites in four different orbits under distinct environmental disturbances, couplings and malicious attacks in NCS is provided for a specific coverage task to describe the design procedure and validate the team formation performance of the optimal H_∞ fault-tolerant decentralized observer-based PID team formation tracking control design under actuator constraint for NCS of LEO satellites.

The main contributions of this work are described as follows:

1. Based on the proposed reference-based feedforward linearization scheme, the team formation tracking control design problem of large-scale LEO satellites can be reformulated as an equivalent linear reference tracking control design problem in (10) for each satellite with an equivalent actuator fault. This problem includes the tracking error of reference-based feedforward linearization, external disturbances, coupling and actuator attack signals. Using the two smoothing methods (14) and (16), or by accounting for equivalent actuator and sensor faults, the fault signals are embedded in the formation tracking error system as an independent linear augmented system of each LEO satellite to avoid corruption and simplify the observer-based team formation tracking control design. Finally, we can employ a linear observer-based PID control scheme in (19) for each LEO satellite to achieve the H_∞ fault-tolerant decentralized observer-based team formation tracking control strategy in (22) for NCS of large-scale LEO satellites.

2. The smoothing signal model is employed to efficiently model fault and attack signals and then is embedded in the augmented team formation tracking error dynamic in (17) of each satellite to avoid their corruptive effect on the estimation of Luenberger observer and PID team formation control in (19) through their precise estimation for the fault and attack signal compensation by the proposed robust H_∞ observer-based decentralized PID team formation control strategy in (22), which is transformed to two LMIs; one LMI in (30) can be solved for PID controller $\bar{K}_i$ and another LMI in (31) can be solved for observer gain L_i for the Luenberger observer-based PID control in (19) for each LEO satellite.

3. The actuator saturation constraints on PID control signals are all transformed to LMIs in (33) for each LEO satellite for more practical PID control designs.

4. The optimal H_∞ fault-tolerant observer-based decentralized PID team formation control design of the NCS of
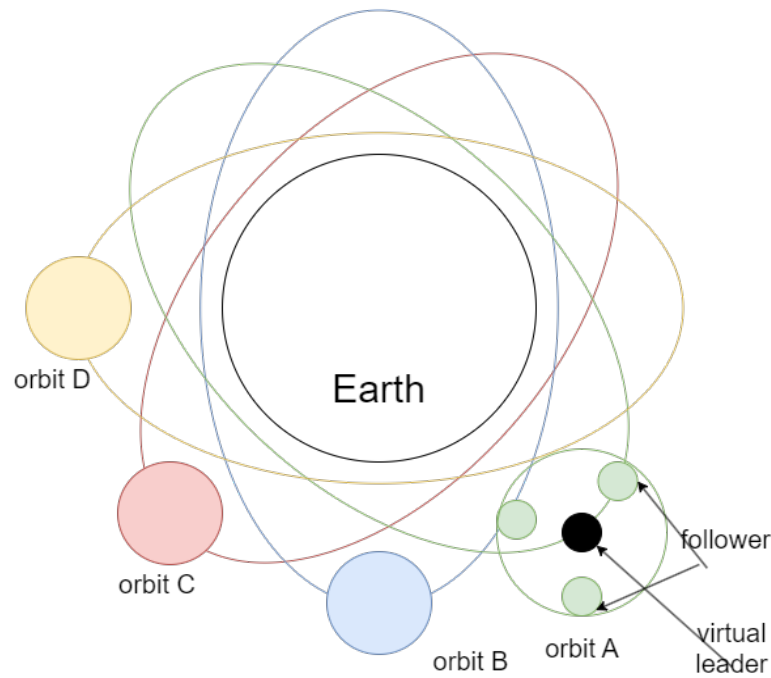
Figure 1. Large-scale satellites with multiple orbits.

large-scale LEO satellites with actuator saturation constraints can be transformed into a three-LMIs-constrained optimization problem in (34) for each satellite in the team. In this way, observer parameters and PID control parameters can be easily obtained by solving the three-LMIs-constrained optimization problem in (34) in a single run using the LMI Toolbox via MATLAB. Therefore, we can avoid the complex parameter tuning process of the conventional PID control design, opening up significant potential for practical applications in the future team formation control designs of large-scale LEO satellites.

The remainder of this paper is organized as follows: In Section 2, the large-scale satellite systems are introduced and the problem formulation of the decentralized robust H_∞ fault-tolerant observer-based PID control for the team formation of NCS of large-scale satellites is presented. An observer-based H_∞ fault-tolerant PID reference tracking control scheme for large-scale LEO satellite team formation NCS with external disturbance and measurement noise is proposed in Section 3. In Section 4, the proposed robust decentralized H_∞ fault-tolerant observer-based PID team formation tracking control design is confirmed by a team formation of 12 LEO satellites in four orbits through a simulation example. Finally, the conclusion is given in Section 5.

2. SYSTEM MODEL AND PROBLEM FORMULATION

2.1. Satellite system model
In this paper, suppose that a team formation control scheme of NCS of large-scale LEO satellites is employed to solve a service problem of satellite coverage, as shown in Figure 1. Therefore, the relative motion dynamic models of satellite altitudes and attitudes are needed first to describe the trajectories of large-scale satellites with a desired team formation as follows:

2.1.1 Relative translation dynamic of satellite system
A large-scale team formation system of LEO satellites in Figure 2 consists of a virtual leader satellite and a group of follower satellites. In Figure 2, the coordinate $[X, Y, Z]$ denotes the Earth-Centered-Inertial (ECI) frame with the origin at the mass center of the Earth, and with X-axis pointing to the direction of the vernal equinox, Z-axis indicating the spin axis of the Earth and Y-axis completing the orthogonal triad. For the satellites, based on the Local-Vertical-Local-Horizontal (LVLH) frame $[x, y, z]$, the relative distance between the virtual leader satellite and a follower satellite can be described, with x-axis representing the orbit direction operation, y-axis pointing to the radial direction, and z-axis standing for the direction orthogonal to other axes. Then, the relative dynamic model of
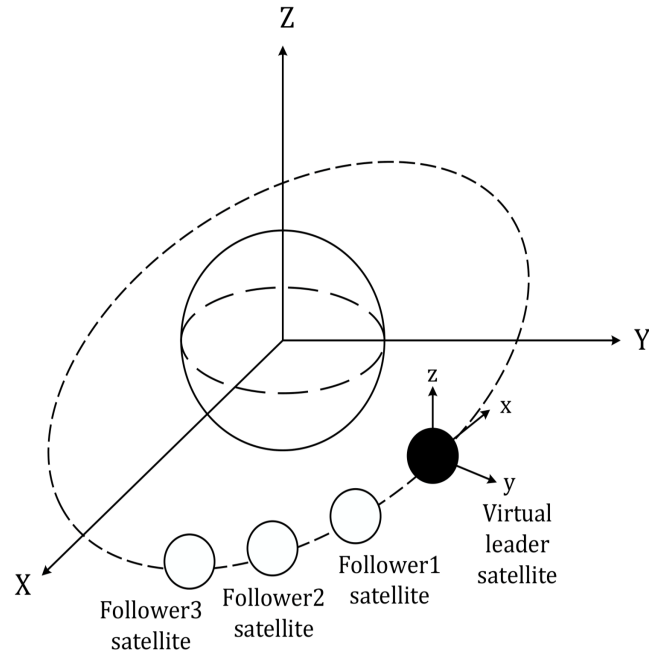
Figure 2. The coordinate frames of a virtual leader satellite and its follower satellite in the team formation.

the *i*th follower satellite to the virtual leader satellite can be given as follows[23]:

$$
\begin{aligned}
\ddot{x}_i &= \dot{v}_{ECI,z_i} y_i + 2v_{ECI,x_i} \dot{y}_i + v_{ECI,z_i}(v_{ECI,z_i} x_i - v_{ECI,x_i} z_i) - \frac{u_e x_i}{R_i^3} + \frac{F_{x_i}}{m_i} + \frac{D_{d_{x_i}}}{m_i} \\
\ddot{y}_i &= v_{ECI,x_i}^2 y_i + 2v_{ECI,x_i} \dot{z}_i + v_{ECI,z_i}^2 y_i - 2v_{ECI,z_i} \dot{x}_i - \dot{v}_{ECI,z_i} x_i + \dot{v}_{ECI,x_i} z_i - \frac{u_e(y_i+R_o)}{R_i^3} + \frac{u_e}{R_o^2} + \frac{F_{y_i}}{m_i} + \frac{D_{d_{y_i}}}{m_i} \\
\ddot{z}_i &= -\dot{v}_{ECI,x_i} y_i - 2v_{ECI,x_i} \dot{y}_i - v_{ECI,x_i}(v_{ECI,z_i} x_i - v_{ECI,x_i} z_i) - \frac{u_e z_i}{R_i^3} + \frac{F_{z_i}}{m_i} + \frac{D_{d_{z_i}}}{m_i} \\
i &= 1, \ldots N
\end{aligned}
\tag{1}
$$

where v_{ECI,x_i} and v_{ECI,z_i} denote the *i*th orbital velocity of the LVLH frame relative to the ECI frame in the X and Z directions, respectively. u_e is the gravitational constant of the Earth. R_o denotes the radial distance from the center of the virtual leader to the Earth and $R_i = \sqrt{x_i^2 + (y_i + R_o)^2 + z_i^2}$ is the distance from the *i*th follower mass center to the Earth. $F_{x_i}, F_{y_i}, F_{z_i}$ denote the control effort on each axis of the *i*th follower satellite and $D_{d_{x_i}}, D_{d_{y_i}}, D_{d_{z_i}}$ are the external disturbance on each axis of the *i*th satellite and m_i is the weight of the *i*th satellite, and N denotes the total number of satellites in the NCS.

2.1.2 Nonlinear attitude dynamic system of satellites
Since the attitude needs to account for the team formation of large-scale satellites, according to the body frame $[b_1^i, b_2^i, b_3^i]$, the orbital reference frame $[o_1^i, o_2^i, o_3^i]$ and ECI frame $[X, Y, Z]$ of the *i*th follower satellite, as shown in Figure 3, the attitude dynamics of the *i*th follower satellite can be obtained by solving[35,36]:

$$
\begin{aligned}
\ddot{\theta}_1^i(t) &= F_{i_1}(t) + \frac{\tau_{\theta_1}^i}{J_1^i} + \frac{D_{\theta_1}^i}{J_1^i} + \sin\theta_2^i \ddot{\theta}_3^i \\
\ddot{\theta}_2^i(t) &= F_{i_2}(t) + \frac{\tau_{\theta_2}^i}{\cos\theta_1^i J_2^i} + \frac{D_{\theta_2}^i}{\cos\theta_1^i J_2^i} - \frac{1}{\cos\theta_1^i}(\cos\theta_2^i \sin\theta_1^i \ddot{\theta}_3^i) \\
\ddot{\theta}_3^i(t) &= F_{i_3}(t) + \frac{\tau_{\theta_3}^i}{\cos\theta_1^i \cos\theta_2^i J_3^i} + \frac{D_{\theta_3}^i}{\cos\theta_1^i \cos\theta_2^i J_3^i} + \frac{1}{\cos\theta_1^i \cos\theta_2^i}(\sin\theta_1^i \ddot{\theta}_2^i) \\
i &= 1, \ldots N
\end{aligned}
\tag{2}
$$

where J_k^i is the inertial principal moment of the *i*th satellite, $\tau_{\theta i}^i$ denotes the control torque, $D_{\theta i}^i$ indicates the external disturbance torque, and $F_{i_k}(t)$ represents the complicated couplings of nonlinear attitude dynamic in the
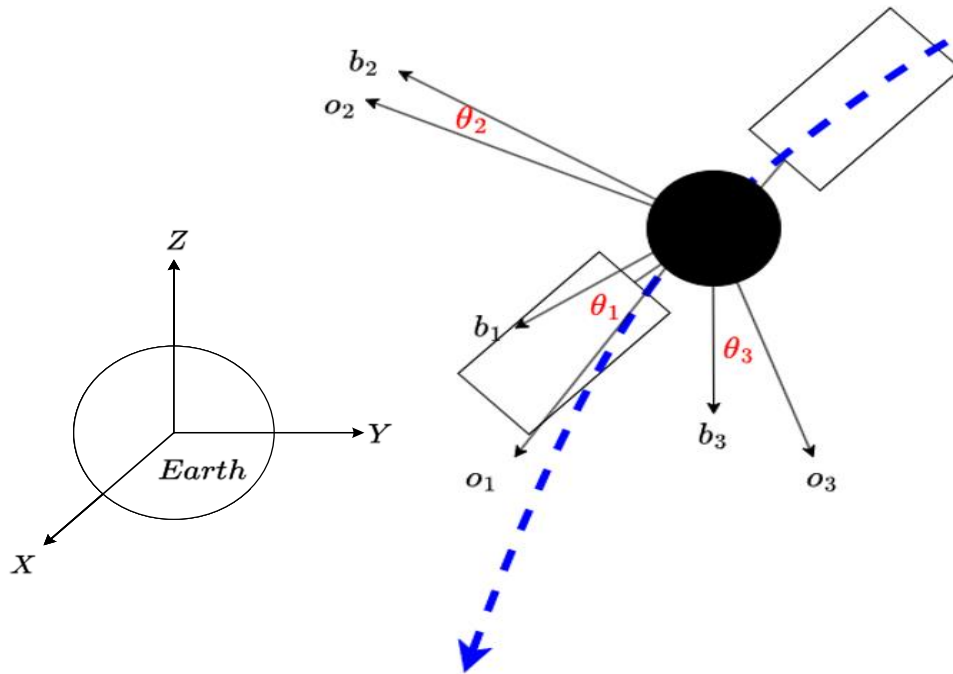
Figure 3. The frames of attitude of the satellite system model

rotation of the *i*th follower satellite for $k = 1, 2, 3$, which consist of a large number of highly nonlinear sinusoidal functions [24,25] and are given as follows:

$$
\begin{aligned}
F_{i_1}(t) =\; & -v_{ECI,z_i}\cos\theta_1^i\sin\theta_3^i\dot\theta_1^i - \cos\theta_3^i\sin\theta_1^i\dot\theta_3^i + \cos\theta_1^i\cos\theta_2^i\cos\theta_3^i\dot\theta_2^i - \cos\theta_3^i\sin\theta_1^i\sin\theta_2^i\dot\theta_1^i - \cos\theta_1^i\sin\theta_2^i\sin\theta_3^i\dot\theta_3^i \\
& + \cos\theta_2^i\dot\theta_3^i\dot\theta_2^i + \cos\theta_3^i\sin\theta_2^i v_{ECI,x_i}\dot\theta_2^i + \cos\theta_2^i\sin\theta_3^i v_{ECI,x_i}\dot\theta_3^i + \sin\theta_1^i\sin\theta_3^i\dot v_{ECI,z_i} - \cos\theta_2^i\cos\theta_3^i\ \dot v_{ECI,x_i} + \cos\theta_1^i\sin\theta_2^i \\
& \times\cos\theta_3^i\dot v_{ECI,z_i} + \frac{(J_2^i - J_3^i)}{J_1^i}\big[-\cos\theta_1^i\sin\theta_1^i\dot\theta_2^i\dot\theta_2^i + \cos\theta_1^i\cos\theta_2^i\cos\theta_1^i\dot\theta_2^i\dot\theta_3^i + v_{ECI,x_i}\cos\theta_1^i\sin\theta_2^i\dot\theta_2^i + v_{ECI,x_i}\cos\theta_2^i\sin\theta_1^i\dot\theta_2^i \\
& + v_{ECI,x_i}\sin\theta_1^i\cos\theta_2^i\sin\theta_3^i\dot\theta_2^i - v_{ECI,x_i}\cos\theta_2^i\cos\theta_2^i\sin\theta_3^i\cos\theta_1^i\dot\theta_3^i - v_{ECI,x_i}v_{ECI,x_i}\cos\theta_2^i\sin\theta_3^i\sin\theta_2^i - v_{ECI,x_i}v_{ECI,z_i} \\
& \times\cos\theta_2^i\sin\theta_3^i\cos\theta_1^i\cos\theta_2^i + \cos\theta_1^i\cos\theta_1^i\cos\theta_2^i v_{ECI,z_i}\dot\theta_2^i - \cos\theta_2^i\sin\theta_1^i\sin\theta_1^i\dot\theta_2^i\dot\theta_3^i + \cos\theta_2^i\cos\theta_2^i\sin\theta_1^i\cos\theta_1^i\dot\theta_3^i\dot\theta_3^i \\
& + v_{ECI,z_i}\cos\theta_2^i\sin\theta_1^i\cos\theta_1^i\cos\theta_2^i\dot\theta_3^i - v_{ECI,z_i}\sin\theta_1^i\sin\theta_1^i\cos\theta_3^i\dot\theta_3^i\dot\theta_2^i - v_{ECI,z_i}\sin\theta_1^i\cos\theta_1^i\sin\theta_2^i\sin\theta_3^i\dot\theta_3^i\dot\theta_2^i + v_{ECI,z_i}\sin\theta_1^i \\
& \times\cos\theta_3^i\cos\theta_2^i\cos\theta_1^i + v_{ECI,z_i}\cos\theta_1^i\cos\theta_2^i\cos\theta_1^i\sin\theta_2^i\sin\theta_3^i + (v_{ECI,z_i})^2\times\sin\theta_1^i\cos\theta_3^i\cos\theta_1^i\cos\theta_2^i + (v_{ECI,z_i})^2\cos\theta_1^i \\
& \times\cos\theta_1^i\cos\theta_2^i\sin\theta_2^i\sin\theta_3^i\big];
\end{aligned}
$$

$$
\begin{aligned}
F_{i_2}(t) =\; & \frac{1}{\cos\theta_1^i}\big[-v_{ECI,z_i}\cos\theta_1^i\cos\theta_3^i\dot\theta_1^i + \sin\theta_1^i\sin\theta_3^i\dot\theta_3^i - \cos\theta_1^i\cos\theta_2^i\sin\theta_3^i\dot\theta_2^i - \cos\theta_1^i\cos\theta_3^i\sin\theta_2^i\dot\theta_3^i + \sin\theta_1^i\sin\theta_2^i\sin\theta_3^i \\
& \times\dot\theta_1^i + \sin\theta_1^i\dot\theta_2^i\dot\theta_1^i - \cos\theta_1^i\cos\theta_2^i\dot\theta_3^i\dot\theta_1^i + \cos\theta_2^i\cos\theta_3^i v_{ECI,x_i}\dot\theta_3^i + \sin\theta_1^i\sin\theta_2^i\dot\theta_3^i\dot\theta_2^i - \sin\theta_2^i\sin\theta_3^i\ v_{ECI,x_i}\dot\theta_2^i + \\
& \cos\theta_2^i\sin\theta_3^i\dot v_{ECI,x_i} \\
& -\sin\theta_1^i\cos\theta_3^i\dot v_{ECI,z_i} - \cos\theta_1^i\sin\theta_2^i\sin\theta_3^i\dot v_{ECI,z_i} + \frac{(J_1^i - J_3^i)}{J_2^i}\big(-\sin\theta_1^i\dot\theta_1^i\dot\theta_2^i + \cos\theta_2^i\cos\theta_1^i\dot\theta_1^i\dot\theta_3^i + v_{ECI,x_i}\sin\theta_2^i\dot\theta_1^i + \\
& v_{ECI,z_i} \\
& \times\cos\theta_1^i\cos\theta_2^i\dot\theta_1^i + \sin\theta_1^i\sin\theta_2^i\dot\theta_2^i\dot\theta_3^i - \sin\theta_2^i\cos\theta_2^i\cos\theta_1^i\dot\theta_3^i\dot\theta_3^i - v_{ECI,x_i}\sin\theta_2^i\sin\theta_2^i\dot\theta_3^i - v_{ECI,z_i}\sin\theta_2^i\cos\theta_1^i\cos\theta_2^i\dot\theta_3^i \\
& -v_{ECI,x_i}\sin\theta_1^i\cos\theta_2^i\cos\theta_3^i\dot\theta_2^i + v_{ECI,x_i}\cos\theta_1^i\cos\theta_2^i\cos\theta_2^i\cos\theta_3^i + (v_{ECI,x_i})^2\cos\theta_2^i\cos\theta_3^i\sin\theta_2^i + v_{ECI,x_i}v_{ECI,z_i}\cos\theta_2^i \\
& \times\cos\theta_3^i\cos\theta_1^i\cos\theta_2^i - v_{ECI,z_i}\sin\theta_1^i\sin\theta_1^i\sin\theta_3^i\dot\theta_2^i + v_{ECI,z_i}\sin\theta_1^i\sin\theta_3^i\cos\theta_2^i\cos\theta_1^i\dot\theta_3^i + v_{ECI,x_i}v_{ECI,z_i}\sin\theta_1^i\sin\theta_2^i\sin\theta_3^i \\
& +(v_{ECI,z_i})^2\sin\theta_1^i\sin\theta_3^i\cos\theta_1^i\cos\theta_2^i + v_{ECI,z_i}\cos\theta_1^i\sin\theta_1^i\sin\theta_2^i\cos\theta_3^i\dot\theta_2^i - v_{ECI,z_i}\cos\theta_1^i\sin\theta_2^i\cos\theta_3^i\cos\theta_1^i\cos\theta_2^i \\
& - v_{ECI,x_i}v_{ECI,z_i}\cos\theta_1^i\sin\theta_2^i\cos\theta_3^i\sin\theta_2^i - (v_{ECI,z_i})^2\cos\theta_1^i\cos\theta_1^i\cos\theta_2^i\sin\theta_2^i\cos\theta_3^i\big)\big];
\end{aligned}
$$

$$
F_{i_3}(t) = \frac{1}{\cos\theta_1^i\cos\theta_2^i}\big[\cos\theta_1^i\dot\theta_1^i\dot\theta_2^i - \cos\theta_2^i v_{ECI,x_i}\dot\theta_2^i + \cos\theta_2^i\sin\theta_1^i\dot\theta_1^i\dot\theta_3^i + \cos\theta_1^i\sin\theta_2^i\dot\theta_2^i\dot\theta_3^i + \cos\theta_2^i\sin\theta_1^i v_{ECI,z_i}\dot\theta_1^i + \cos\theta_1^i
$$

$\times \sin \theta_2^i v_{ECI,z_i} \dot{\theta}_2^i + \sin \theta_2^i \dot{v}_{ECI,x_i} + \cos \theta_1^i \cos \theta_2^i \dot{v}_{ECI,z_i} + \frac{(J_2^i - J_1^i)}{J_3^i}(\cos \theta_1^i \dot{\theta}_1^i \dot{\theta}_2^i + \cos \theta_2^i \sin \theta_1^i - v_{ECI,x_i} \cos \theta_2^i \sin \theta_3^i \dot{\theta}_1^i$

$+ v_{ECI,z_i} \sin \theta_1^i \cos \theta_3^i \dot{\theta}_1^i + v_{ECI,z_i} \cos \theta_1^i \sin \theta_2^i \sin \theta_3^i \dot{\theta}_1^i - \sin \theta_2^i \cos \theta_1^i \dot{\theta}_2^i \dot{\theta}_3^i - \sin \theta_2^i \sin \theta_1^i \cos \theta_2^i \dot{\theta}_3^i \dot{\theta}_3^i + v_{ECI,x_i} \sin \theta_2^i \cos \theta_2^i$
$\times \sin \theta_3^i \dot{\theta}_3^i - v_{ECI,z_i} \sin \theta_1^i \cos \theta_3^i \sin \theta_2^i \dot{\theta}_3^i - v_{ECI,z_i} \cos \theta_1^i \sin \theta_2^i \sin \theta_3^i \sin \theta_2^i \dot{\theta}_3^i + v_{ECI,x_i} \cos \theta_2^i \cos \theta_3^i \cos \theta_1^i \dot{\theta}_2^i +$
v_{ECI,x_i}
$\times \cos \theta_2^i \cos \theta_3^i \cos \theta_2^i \sin \theta_1^i \dot{\theta}_3^i - (v_{ECI,x_i})^2 \cos \theta_2^i \cos \theta_3^i \cos \theta_2^i \sin \theta_3^i + v_{ECI,x_i} v_{ECI,z_i} \cos \theta_2^i \sin \theta_1^i \cos \theta_3^i \cos \theta_3^i +$
v_{ECI,x_i}
$\times v_{ECI,z_i} \cos \theta_2^i \cos \theta_3^i \cos \theta_1^i \sin \theta_2^i \sin \theta_3^i - v_{ECI,z_i} \sin \theta_1^i \sin \theta_3^i \cos \theta_1^i \dot{\theta}_2^i - v_{ECI,z_i} \cos \theta_1^i \sin \theta_2^i \cos \theta_3^i \cos \theta_2^i \sin \theta_1^i \dot{\theta}_3^i$
$+ v_{ECI,x_i} v_{ECI,z_i} \cos \theta_1^i \sin \theta_2^i \cos \theta_3^i \cos \theta_2^i \sin \theta_3^i - (v_{ECI,z_i})^2 \cos \theta_1^i \sin \theta_2^i \cos \theta_3^i \sin \theta_1^i \cos \theta_3^i - (v_{ECI,z_i})^2 \cos \theta_1^i \sin \theta_2^i$
$\times \cos \theta_3^i \cos \theta_1^i \sin \theta_2^i \sin \theta_3^i)];$

Assumption 1 In this study, the orbit reference frame in the attitude dynamic model of LEO satellites is the same as the LVLH reference model in the relative translation dynamic model [25].

2.2 Problem formulation

Given the Newton-Euler equations in (1) and (2), the relative altitude and attitude dynamic models of each follower satellite in the team formation are highly complex and nonlinear. These models can be combined into the following nonlinear dynamic system of each LEO satellite with control input $u_i(t)$, coupling effect $c_{ij}(t)$ from other satellites and external disturbance $d_i(t)$:

$$M_i \ddot{q}_i(t) + H(q_i(t), \dot{q}_i(t)) = u_i(t) + \sum_{\substack{j \neq i}}^{N} c_{ij}(t) + d_i(t) \qquad i = 1, ..., N \qquad (3)$$

where $q_i(t) = \begin{bmatrix} x_i(t) & y_i(t) & z_i(t) & \theta_1^i(t) & \theta_2^i(t) & \theta_3^i(t) \end{bmatrix}^T$, $M_i = diag[m_i, m_i, m_i, J_1^i, J_2^i, J_3^i]$,

$H(q_i(t), \dot{q}_i(t)) = \begin{bmatrix} 0 & 0 & 0 & J_1^i F_{i_1} & J_2^i F_{i_2} & J_3^i F_{i_3} \end{bmatrix}^T - m \begin{bmatrix} V_1 & O \\ O & O \end{bmatrix} q_i(t) - m \begin{bmatrix} V_2 & O \\ O & O \end{bmatrix} \dot{q}_i(t),$

$$V_1 = \begin{bmatrix} v_{ECI,z_i}^2 & \dot{v}_{ECI,z_i} & v_{ECI,x_i} v_{ECI,z_i} \\ -\dot{v}_{ECI,z_i} & v_{ECI,x_i}^2 + v_{ECI,z_i}^2 & \dot{v}_{ECI,x_i} \\ -v_{ECI,x_i} v_{ECI,z_i} & -\dot{v}_{ECI,z_i} & v_{ECI,x_i}^2 \end{bmatrix}, V_2 = \begin{bmatrix} 0 & 2v_{ECI,x_i} & 0 \\ -2v_{ECI,z_i} & 0 & 2v_{ECI,x_i} \\ 0 & -2v_{ECI,x_i} & 0 \end{bmatrix},$$

$$u_i(t) = diag[1, 1, 1, 1, \frac{1}{\cos \theta_1^i(t)}, \frac{1}{\cos \theta_1^i(t) \cos \theta_2^i(t)}] \times [F_{x_i}, F_{y_i}, F_{z_i}, \tau_{\theta i}^1, \tau_{\theta i}^2, \tau_{\theta i}^3]^T$$

$u_i(t) \in \mathbb{R}^6$ is the control input, $q_i(t) \in \mathbb{R}^6$ is the state vector, $M_i \in \mathbb{R}^{6 \times 6}$ is the inertia matrix, $H(q_i(t), \dot{q}_i(t)) \in \mathbb{R}^6$ is the non-inertial force vector and $c_{ij}(t) \in \mathbb{R}^6$ denotes the coupling from the jth satellite to the ith satellite via CCI.

To let N satellites maintain a specific time-varying formation shape during the operating, the virtual leader method is considered in this paper. The team formation shape of N LEO satellites is constructed by a virtual leader and N follower satellites and the N followers will track the virtual leader's trajectory with a specific time-varying team formation shape $(r_1^T(t), ... r_i^T(t), ... r_N^T(t))^T$ to achieve a desired team formation for a coverage task. Based on the feedforward linearization control scheme, the following reference-based feedforward linearization control law is considered for each satellite system in the team formation:

$$u_i(t) = M_i(u_{pid,i}(t) + \ddot{r}_i(t)) + H(r_i(t), \dot{r}_i(t)) \qquad (4)$$

where $r_i(t) \in \mathbb{R}^6$ is the target reference trajectory of the ith LEO satellite, M_i, $\ddot{r}_i(t)$ and $H(r_i(t), \dot{r}_i(t))$ are the reference-based feedforward control terms to be employed to eliminate the nonlinearity of each LEO satellite system to achieve the feedforward linearization in the sequel, and $u_{pid,i}(t)$ is the PID controller of the ith LEO satellite in the team, which will be further designed for enhancing the robust team formation tracking performance of large-scale LEO satellites.

Assumption 2 In the team formation, the virtual leader information is always available for each follower satellite [24,25].

Given the widespread utilization of conventional PID controllers across various industrial automatic process control applications, this study also leverages these controllers to govern individual satellites to attain the desired team formation. The conventional PID control for the ith satellite is given as follows:

$$u_{pid}(t) = K_{i,P}e_i(t) + K_{i,I}\int_0^t e_i(\tau)d\tau + K_{i,D}\frac{de_i(t)}{dt} \qquad i = 1, ...N \qquad (5)$$

where $K_{i,P} \in \mathbb{R}^{6\times6}, K_{i,I} \in \mathbb{R}^{6\times6}, K_{i,D} \in \mathbb{R}^{6\times6}$ are the controller gains with respect to the PID controller, $e_i(t) = q_i(t) - r_i(t) \in \mathbb{R}^6$ denotes the formation tracking error of the positions and attitude of the ith satellite.

Nevertheless, traditional PID control techniques have their restrictions, primarily applying to linear or uncomplicated nonlinear dynamic systems. Hence, there is a need to enhance the conventional PID control approach to address the intricate decentralized H_∞ team formation tracking control design challenges encountered in highly nonlinear dynamic satellite NCSs, as illustrated in Figure 4. This study introduces the utilization of coordinate transformation to enable a systematic analysis and design of the conventional PID control scheme for large-scale, highly nonlinear LEO satellite systems, focusing on the decentralized H_∞ fault-tolerant team formation tracking control. In order to simplify the parameter tuning problem of a PID controller, the controller $u_{pid}(t)$ for each LEO satellite in (5) is reformulated as follows:

$$u_{pid}(t) = K_{i,P}e_i(t) + K_{i,I}\int_0^t e_i(\tau)d\tau + K_{i,D}\frac{de_i(t)}{dt} = \begin{bmatrix} K_{i,I} & K_{i,P} & K_{i,D} \end{bmatrix}\begin{bmatrix} \int_0^t e_i(\tau)d\tau \\ e_i(t) \\ \frac{de_i(t)}{dt} \end{bmatrix}$$

$$= K_iE_i(t) \qquad\qquad\qquad (6)$$

with $K_i = \begin{bmatrix} K_{i,I} & K_{i,P} & K_{i,D} \end{bmatrix}$ and $E_i(t) = \begin{bmatrix} \int_0^t e_i(\tau)d\tau \\ e_i(t) \\ \frac{de_i(t)}{dt} \end{bmatrix}$

3. ROBUST H∞ OBSERVER-BASED PID FAULT-TOLERANT DECENTRALIZED CONTROL OF NCS OF TEAM FORMATION OF LARGE-SCALE LEO SATELLITES

In this research, the configuration of the team formation observer-based PID control of NCS of N satellites is shown in Figure 4 via a wireless communication network. In practical applications, the NCS of a team formation of large-scale LEO satellites will suffer from actuator and sensor malicious attacks via a wireless communication network, as shown in Figure 4. The dynamic model of each satellite in the team formation NCS in Figure 4 is given as follows:

$$M_i\ddot{q}_i(t) + H(q_i(t), \dot{q}_i(t)) = u_i(t) + \sum_{j\neq i}^N c_{ij}(t) + a_i(t) + d_i(t) \qquad (7)$$

$$y_i(t) = C_iX_i(t) + D_i(s_i(t) + n_i(t))$$

where $X_i(t) = [\int_0^t q_i(\tau)d\tau^T q_i(t)^T \dot{q}_i(t)^T]^T \in \mathbb{R}^{18}$, $C_i \in \mathbb{R}^{6\times18}$ is the measurement output matrix, $y_i(t) \in \mathbb{R}^6$ is the output vector. $a_i(t)$ and $s_i(t)$ denote the actuator and sensor malicious attack signal through wireless network communication, respectively, D_i is the sensor fault matrix, and $n_i(t)$ denotes the measurement output noise.

Assumption 3 Actuator attack signal, sensor attack signal and external disturbance [24,25], $a_i(t)$, $s_i(t)$ and $d_i(t)$ *are of finite energy, i.e.,* $a_i(t)$, $s_i(t)$ and $d_i(t) \in L_2[0, \infty)$.

Now, substituting the control law $u_i(t)$ in (4) into (7), we have:

$$M_i(\ddot{q}_i(t) - \ddot{r}_i(t)) = M_iu_{pid,i}(t) - \Delta H_i(t) + \sum_{j\neq i}^N c_{ij}(t) + a_i(t) + d_i(t) \qquad (8)$$
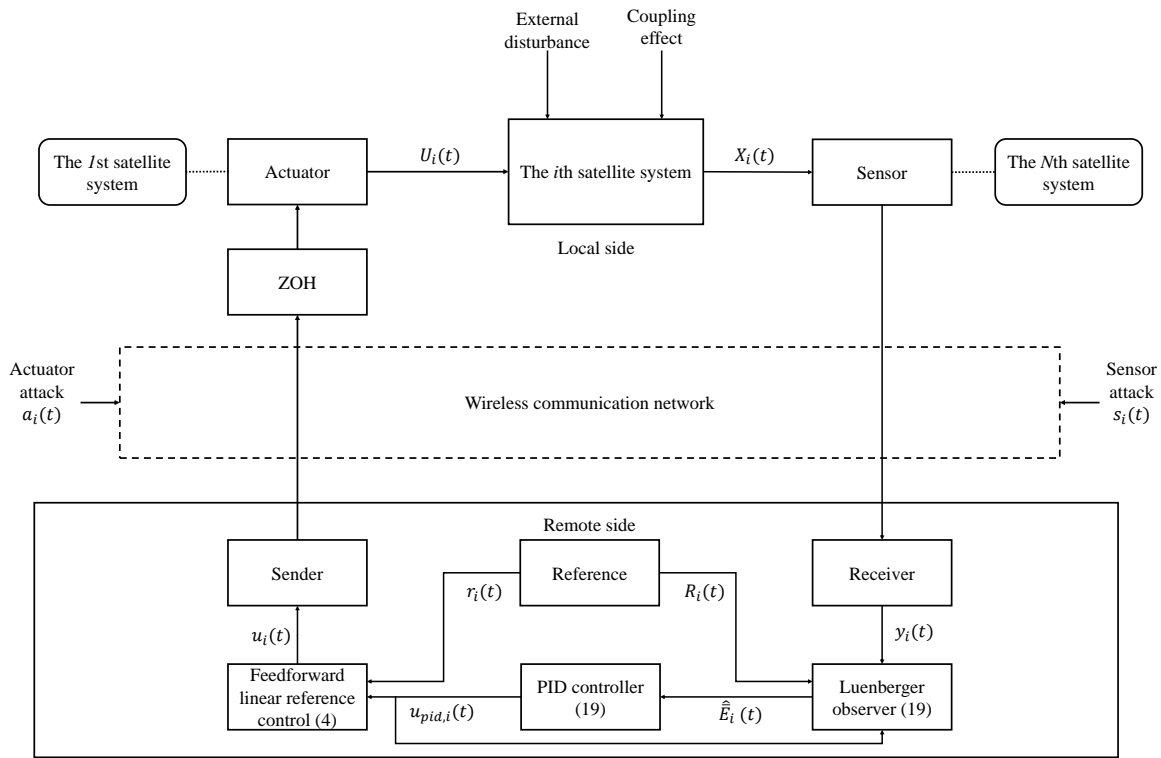
Figure 4. The observer-based PID team formation control of NCS of N satellites, where $u_{pid,i}(t)$ denotes the PID control in (6), $u_i(t)$ denotes the feedforward linearization reference control in (4) and $U_i(t)$ is the actual control on the ith satellite system from the actuator. $a_i(t)$ and $s_i(t)$ denote the actuator and sensor attack signals via a wireless communication network, respectively.

with $\Delta H_i(t) = H(q_i(t), \dot{q}_i(t)) - H(r_i(t), \dot{r}_i(t))$ as the error term from reference-based feedforward linearization. By multiplying M_i^{-1} on both sides of (8) and after some adjustment, the differential of formation tracking errors of the ith satellite is obtained as follows:

$$\ddot{e}_i(t) = u_{pid,i}(t) + f_{a,i}(t) \tag{9}$$

where $f_{a,i}(t) = M_i^{-1}(-\Delta H_i(t) + \sum_{j \neq i}^{N} c_{ij}(t) + a_i(t) + d_i(t)) \in \mathbb{R}^6$ is considered as an equivalent actuator fault signal of PID controller. Since the sensor information will be transmitted back to the ground station for calculating control command through the network communication channel of satellites, not only the sensor noise but also the cyber-attack signal are concerned. So, to simplify the design procedure, we can rewrite the formation tracking error of each LEO satellite as the following linear system:

$$\begin{aligned} \dot{E}_i(t) &= A_i E_i(t) + B_i(u_{pid,i}(t) + f_{a,i}(t)) \\ y_i(t) &= C_i X_i(t) + D_i f_{s,i}(t) \end{aligned} \tag{10}$$

where $E_i(t) = \begin{bmatrix} \int_0^t e_i(\tau)d\tau \\ e_i(t) \\ \frac{de_i(t)}{dt} \end{bmatrix}$, $A_i = \begin{bmatrix} O & I_6 & O \\ O & O & I_6 \\ O & O & O \end{bmatrix}$, $B_i = \begin{bmatrix} O \\ O \\ I_6 \end{bmatrix}$, the equivalent sensor fault signal $f_{s,i}(t) = s_i(t) + n_i(t)$.

Then, we define $R_i(t) = [\int_0^t r_i(\tau)d\tau^T r_i(t)^T \dot{r}_i(t)^T]^T$ so that we can rewrite (10) as:

$$\begin{aligned} \dot{E}_i(t) &= A_i E_i(t) + B_i(u_{pid,i}(t) + f_{a,i}(t)) \\ y_i(t) &= C_i E_i(t) + C_i R_i(t) + D_i f_{s,i}(t) \end{aligned} \tag{11}$$

In this study, to estimate fault signals by the following traditional for the equivalent actuator and sensor observer for

the FTC design, a novel dynamic smoothing model is proposed for the equivalent actuator and sensor fault signals $f_{a,i}(t)$ and $f_{s,i}(t)$. First, based on the derivative definition of $\dot{f}_{a,i}(t) = \lim_{h\to 0} \frac{f_{a,i}(t+h) - f_{a,i}(t)}{h}$, the smoothing model of $f_{a,i}(t)$ is given as follows:

$$\dot{f}_{a,i}(t) = \frac{1}{h}(f_{a,i}(t+h) - f_{a,i}(t)) + \epsilon_{1,ai}(t),$$

$$\dot{f}_{a,i}(t-h) = \frac{1}{h}(f_{a,i}(t) - f_{a,i}(t-h)) + \epsilon_{2,ai}(t),$$

$$\vdots$$

$$\dot{f}_{a,i}(t - k_a h) = \frac{1}{h}(f_{a,i}(t - (k_a - 1)h) - f_{a,i}(t - k_a h) + \epsilon_{k,ai}(t) \tag{12}$$

where $\epsilon_{1,a,i}(t), ..., \epsilon_{k_a,a,i}(t)$ denote approximation errors of the derivative at different smoothing time points for actuator fault signal $f_{a,i}(t)$. The constant $h > 0$ denotes a small time interval, $k_a \in \mathbb{N}$ represents the number of actuator fault signal smoothing steps. By the extrapolation scheme [37], the next fault signal $f_{a,i}(t+h)$ in (12) can be predicted as follows:

$$f_{a,i}(t+h) = \sum_{j=0}^{k_a} a_j f_{a,i}(t - jh) + \delta_{a,i}(t) \tag{13}$$

where a_j, $j = 0, ...k_a$ are the extrapolation coefficients and $\delta_{a,i}(t)$ denotes the extrapolation error of $f_{a,i}(t+h)$. Then, the smoothing model of actuator fault signal $f_{a,i}(t)$ is obtained:

$$\begin{aligned} \dot{F}_{a,i}(t) &= A_{a,i}F_{a,i}(t) + v_{a,i}(t) \\ f_{a,i}(t) &= Z_{a,i}F_{a,i}(t) \end{aligned} \tag{14}$$

where $F_{a,i}(t) = [f_{a,i}^T(t), f_{a,i}^T(t-h), ..., f_{a,i}^T(t - (k_a - 1)h), f_{a,i}^T(t - k_a h)]^T$, the smoothed model error of actuator $v_{a,i}(t) = [(\epsilon_{1,ai}(t) + \delta_{a,i}(t)/h)^T, \epsilon_{2,ai}^T(t), ..., \epsilon_{k_a,ai}^T(t)]^T$, $Z_{a,i} = [1, 0, ..., 0] \otimes I_n$ where n is the window size of smoothing signal model and

$$A_{a,i} = \begin{bmatrix} \frac{-1+a_0}{h}I_n & \frac{a_1}{h}I_n & \frac{a_2}{h}I_n & \cdots & \frac{a_{k_a}}{h}I_n \\ \frac{1}{h}I_n & -\frac{1}{h}I_n & O & \cdots & O \\ O & \frac{1}{h}I_n & -\frac{1}{h}I_n & \cdots & O \\ \vdots & & \vdots & \ddots & \vdots \\ O & \cdots & O & \frac{1}{h}I_n & -\frac{1}{h}I_n \end{bmatrix}$$

In the same way, we could extrapolate the future sensor fault signal $f_{s,i}(t+h)$ as follows:

$$f_{s,i}(t+h) = \sum_{l=0}^{k_s} b_l f_{s,i}(t - jh) + \delta_{s,i}(t) \tag{15}$$

where b_l, $l = 0, ...k_s$ are the extrapolation coefficients, $\delta_{s,i}(t)$ denotes the extrapolation error of $f_{s,i}(t+h)$. Then, the following smoothing model of sensor fault signal $f_{s,i}(t)$ is obtained:

$$\begin{aligned} \dot{F}_{s,i}(t) &= A_{s,i}F_{s,i}(t) + v_{s,i}(t) \\ f_{s,i}(t) &= Z_{s,i}F_{s,i}(t) \end{aligned} \tag{16}$$

where $F_{s,i}(t) = [f_{s,i}^T(t), f_{s,i}^T(t-h), ..., f_{s,i}^T(t - (k_s - 1)h), f_{s,i}^T(t - k_s h)]^T$, the smoothing model error of sensor $v_{s,i}(t) = [(\epsilon_{1,si}(t) + \delta_{s,i}(t)/h)^T, \epsilon_{2,si}^T(t), ..., \epsilon_{k_s,si}^T(t)]^T$, $Z_{s,i} = [1, 0, ..., 0] \otimes I_m$ where m is the window size of smoothing signal model and

$$A_{s,i} = \begin{bmatrix} \frac{-1+b_0}{h}I_m & \frac{b_1}{h}I_m & \frac{b_2}{h}I_m & \cdots & \frac{b_{k_s}}{h}I_m \\ \frac{1}{h}I_m & -\frac{1}{h}I_m & O & \cdots & O \\ O & \frac{1}{h}I_m & -\frac{1}{h}I_m & \cdots & O \\ \vdots & & \vdots & \ddots & \vdots \\ O & \cdots & O & \frac{1}{h}I_m & -\frac{1}{h}I_m \end{bmatrix}$$

Embedding (14) and (16) into (11), we get the following linear decoupled augmented tracking error system of each satellite:

$$\dot{\bar{E}}_i(t) = \bar{A}_i \bar{E}_i(t) + \bar{B}_i u_{pid,i}(t) + \bar{v}_i(t)$$
$$y_i(t) = \bar{C}_i \bar{E}_i(t) + C_i R_i(t) \tag{17}$$

Where $\bar{E}_i(t) = \begin{bmatrix} E_i(t) \\ F_{a,i}(t) \\ F_{s,i}(t) \end{bmatrix}$ is the augmented tracking error vector, $\bar{A}_i = \begin{bmatrix} A_i & B_i Z_{a,i} & O \\ O & A_{a,i} & O \\ O & O & A_{s,i} \end{bmatrix}$, $\bar{B}_i = \begin{bmatrix} B_i \\ O \\ O \end{bmatrix}$, $\bar{C}_i =$

$\begin{bmatrix} C_i & O & D_i Z_{s,i} \end{bmatrix}$, and $\bar{v}_i(t) = \begin{bmatrix} O \\ v_{a,i}(t) \\ v_{s,i}(t) \end{bmatrix}$. It can be seen that the fault signals $f_{a,i}(t)$ and $f_{s,i}(t)$ in (10) are embedded in $\bar{E}_i(t)$ to be estimated for compensation control to avoid corruption on the team formation observer-based PID control of each LEO satellite in the sequel.

Assumption 4 The augmented tracking error system in (17) is observable, i.e.,

$$rank \begin{bmatrix} zI - \bar{A}_i \\ \bar{C}_i \end{bmatrix} = 3 \times 6 + (k_a + 1)n + (k_s + 1)m \quad \forall z \in eig(\bar{A}_i) \tag{18}$$

that is, the dimension of $\bar{A}_i = 3 \times 6 + (k_a + 1)n + (k_s + 1)m$ is the total dimension of A_i, $A_{a,i}$ and $A_{s,i}$.

Remark 1 In order to satisfy the observability condition in (18), the extrapolation coefficients $a_0, ...a_j, ...a_{ka}$ and $b_0, ...b_l, ...b_{ks}$ should be specified so that $A_{a,i}$ in (14) and $A_{s,i}$ in (16) have not any common eigenvalue.

Because the fault signals are embedded into a state vector of the augmented tracking error system in (17), we can not only estimate them by a Luenberger observer but also compensate the corruption effect of these fault signals by a PID controller. The following fault-tolerant Luenberger observer-based PID controller is proposed, at the remote side in Figure 4, to accomplish an active decentralized H∞ team formation FTC of the NCS of LEO satellites:

$$\dot{\hat{\bar{E}}}_i(t) = \bar{A}_i \hat{\bar{E}}_i(t) + \bar{B}_i u_{pid,i}(t) - L_i(y_i(t) - \hat{y}_i(t))$$
$$u_{pid,i}(t) = \bar{K}_i \hat{\bar{E}}_i(t) \tag{19}$$

where $\hat{y}_i(t) = \bar{C}_i \hat{\bar{E}}_i(t) + C_i R_i(t)$.

Remark 2 From (6), the fault-tolerant observer-based PID controller is given by $u_{pid,i}(t) = \bar{K}_i \hat{\bar{E}}_i(t) = [K_i, K_{Fai}, K_{Fsi}][\hat{E}_i^T(t), \hat{F}_{a,i}^T(t), \hat{F}_{s,i}^T(t)]^T$, where the estimated fault signals $\hat{F}_{a,i}^T(t)$ and $\hat{F}_{s,i}^T(t)$ are fed back to compensate for fault signals $f_{a,i}(t)$ and $f_{s,i}(t)$ in (10). This fault-tolerant observer-based PID control law $u_{pid,i}(t)$, as shown in (19), combines both fault-tolerant capability and PID control functionality.

Let $\tilde{E}_i(t) = \bar{E}_i(t) - \hat{\bar{E}}_i(t)$; then, the augmented estimation error system of Luenberger observer can be obtained from (17) and (19) as follows:

$$\dot{\tilde{E}}_i(t) = \bar{A}_i \tilde{E}_i(t) + L_i \bar{C}_i \tilde{E}_i(t) + \bar{v}_i(t)$$
$$= (\bar{A}_i + L_i \bar{C}_i) \tilde{E}_i(t) + \bar{v}_i(t) \tag{20}$$

Combining (17), (19) and (20), we can get the following augmented reference tracking and estimation error system of each satellite:

$$\dot{\tilde{S}}_i(t) = \tilde{A}_i \tilde{S}_i(t) + \tilde{v}_i(t) \tag{21}$$

where $\tilde{S}_i(t) = \begin{bmatrix} \bar{E}_i(t) \\ \tilde{E}_i(t) \end{bmatrix}$, $\tilde{A}_i = \begin{bmatrix} \bar{A}_i + \bar{B}_i \bar{K}_i & -\bar{B}_i \bar{K}_i \\ O & \bar{A}_i + L_i \bar{C}_i \end{bmatrix}$, and $\tilde{v}_i(t) = \begin{bmatrix} \bar{v}_i(t) \\ \bar{v}_i(t) \end{bmatrix}$

To specify PID control gains $\bar{K}_i$ and observer gains L_i in (19) to accomplish a robust estimation and tracking performance for the augmented system in (21) with disturbance $\tilde{v}(t)$, the H_∞ robust fault-tolerant observer-based decentralized PID team formation tracking control strategy for the NCS of LEO satellites below a prescribed disturbance attenuation level ρ_i for each satellite is proposed as follows:

$$\frac{\int_0^{t_f} (\bar{E}_i^T(t)Q_{i1}\bar{E}_i(t) + \tilde{E}_i^T(t)Q_{i2}\tilde{E}_i(t) + u_{pid,i}^T(t)R_i u_{pid,i}(t))dt - V(\tilde{S}_i(0))}{\int_0^{t_f} \tilde{v}_i^T(t)\tilde{v}_i(t)dt} \leq \rho_i^2, i = 1, \ldots, N. \quad (22)$$

$\forall \tilde{v}_i(t) \in L_2[0, \infty)$, where t_f is the terminal time, $Q_{i1} \geq 0, Q_{i2} \geq 0, R_i > 0$ are respectively the weighting matrix of tracking error, estimation error and control input, $V(\tilde{S}_i(0))$ is the initial condition effect on the augmented tracking and estimation error system in (21), and $\tilde{v}_i(t)$ is the total error term that needs to be attenuated.

If we can find the PID control gain $\bar{K}_i$ and the observer gain L_i in (19) such that (22) holds, then the total error term effect $\tilde{v}_i(t)$ on the augmented tracking error $\bar{E}_i(t)$ and the augmented estimation error $\tilde{E}_i(t)$ can be less than a prescribed level ρ_i^2 from the viewpoint of energy. Before solving the H_∞ robust fault-tolerant observer-based decentralized PID team formation tracking control design problem of large-scale LEO satellites in (22), the following two lemmas are given:

Lemma 1 For any matrices A and B with appropriate dimensions and matrix $X = X^T > 0$, the following inequality holds[38] :

$$A^T B + B^T A \leq A^T X^{-1} A + B^T X B \quad (23)$$

Lemma 2 (Schur Complement[38]) For the matrices $A = A^T, B = B^T$ and matrix X with appropriate dimensions, the following statement is true:

$$\begin{bmatrix} A & X \\ X^T & B \end{bmatrix} > 0 \Leftrightarrow B > 0, A - XB^{-1}X^T > 0 \quad (24)$$

Then, the following theorem is proposed:

Theorem 1 (i) If there exist matrices $P_i = P_i^T > 0, \bar{K}_i, L_i$ such that the following Riccati-like matrix inequalities hold:

$$Q_i + P_i\tilde{A}_i + \tilde{A}_i^T P_i + \tilde{K}_i^T R_i \tilde{K}_i + \frac{1}{\rho_i^2} P_i P_i \leq 0, \ i = 1, ..., N \quad (25)$$

where $\tilde{K}_i = \begin{bmatrix} \bar{K}_i & -\bar{K}_i \end{bmatrix}$, $Q_i = \begin{bmatrix} Q_{i1} & 0 \\ 0 & Q_{i2} \end{bmatrix}$, then the robust H_∞ fault-tolerant decentralized observer-based PID team formation control strategy in (22) of each satellite of NCS of LEO satellites can be achieved.
(ii) If $\tilde{v}_i(t) \in L_2[0, \infty)$, then $\bar{E}_i(t) \to 0, \tilde{E}_i(t) \to 0$ and $u_{pid,i}(t) \to 0$ quadratically as $t \to \infty$ for each LEO satellite NCS of the large-scale team formation of LEO satellites.

Proof. (i) Choose the Lyapunov function $V(\tilde{S}_i(t)) = \tilde{S}_i^T(t)P_i\tilde{S}_i(t)$ for the augmented system (21) with $P_i = P_i^T > 0$, we have:

$$\int_0^{t_f} (\tilde{S}_i^T(t)Q_i\tilde{S}_i(t) + u_{pid,i}^T(t)R_i u_{pid,i}(t))dt$$

$$= V(\tilde{S}_i(0)) - V(\tilde{S}_i(t_f)) + \int_0^{t_f} (\tilde{S}_i^T(t)Q_i\tilde{S}_i(t) + u_{pid,i}^T(t)R_i u_{pid,i}(t) + \dot{V}(\tilde{S}_i(t)))dt \quad (26)$$

$$\leq V(\tilde{S}_i(0)) + \int_0^{t_f} (\tilde{S}_i^T(t)Q_i\tilde{S}_i(t) + u_{pid,i}^T(t)R_i u_{pid,i}(t) + \dot{\tilde{S}}_i^T(t)P_i\tilde{S}_i(t) + (\dot{\tilde{S}}_i^T(t)P_i\tilde{S}_i(t))^T)dt$$

By (21) and Lemma 1, we have:

$$\dot{\tilde{S}}_i^T(t)P_i\tilde{S}_i(t) + (\dot{\tilde{S}}_i^T(t)P_i\tilde{S}_i(t))^T$$

$$= (\tilde{A}_i\tilde{S}_i(t) + \tilde{v}_i(t))^T P\tilde{S}_i(t) + ((\tilde{A}_i\tilde{S}_i(t) + \tilde{v}_i(t))^T P\tilde{S}_i(t))^T \quad (27)$$

$$\leq \tilde{S}_i^T(t)(P_i\tilde{A}_i + \tilde{A}_i^T P_i + \frac{1}{\rho_i^2}P_i P_i)\tilde{S}_i(t) + \rho_i^2 \tilde{v}_i^T(t)\tilde{v}_i(t)$$

Substituting (19), (27) and $\tilde{S}_i^T(t)Q_i\tilde{S}_i(t) = \bar{E}_i^T(t)Q_{i1}\bar{E}_i(t) + \tilde{E}_i^T(t)Q_{i2}\tilde{E}_i(t)$ into (26), we get:

$$
\int_0^{t_f} (\bar{E}_i^T(t)Q_{i1}\bar{E}_i(t) + \tilde{E}_i^T(t)Q_{i2}\tilde{E}_i(t)dt + u_{pid,i}^T(t)R_i u_{pid,i}(t))dt
$$
$$
\leq V(\tilde{S}_i(0)) + \int_0^{t_f} (\tilde{S}_i^T(t)(Q_i + P_i\tilde{A}_i + \tilde{A}_i^T P_i + \tilde{K}_i^T R_i \tilde{K}_i + \frac{1}{\rho_i^2}P_i P_i)\tilde{S}_i(t) + \rho_i^2 \tilde{v}_i^T(t)\tilde{v}_i(t))dt
$$
(28)

Thus, if (25) holds, (22) also holds.

(ii) If $\tilde{v}_i(t) \in L_2[0, \infty)$, since $V(\tilde{S}_i(0))$ and $\int_0^\infty \tilde{v}_i^T(t)\tilde{v}_i(t)dt < \infty$, then from (28) we get $\int_0^{t_f}(\bar{E}_i^T(t)Q_{i1}\bar{E}_i(t) + \tilde{E}_i^T(t)Q_{i2}\tilde{E}_i(t)dt + u_{pid,i}^T(t)R_i u_{pid,i}(t))dt \leq V(\tilde{S}_i(0)) + \rho_i \int_0^{t_f} \tilde{v}_i^T(t)\tilde{v}_i(t)dt < \infty$. It implies that, $\lim_{t \to \infty} \bar{E}_i^T(t)\bar{E}_i(t) \to 0$, $\tilde{E}_i^T(t)\tilde{E}_i(t) \to 0$ and $u_{pid,i}^T(t)u_{pid,i}(t) \to 0$ as $t_f \to \infty$ ∎

Although the Riccati-like matrix inequalities in (25) for the existence of the H_∞ decentralized fault-tolerant observer-based PID tracking control strategy in (22) have been derived, they cannot be easily solved because they represent a bilinear matrix inequality (BMI). Additionally, strong coupling exists between the designed variables P_i, $\bar{K}_i$ and L_i [39]. Therefore, a two-step design procedure is developed to solve BMI in (25) by two corresponding LMIs as follows:

Step 1: To begin with, let the Lyapunov energy function of the augmented system in (21) be the sum of two Lyapunov functions of two subsystems (17) and (20), i.e., $V(\tilde{S}_i(t)) = \tilde{S}_i^T(t)P_i\tilde{S}_i(t) = \bar{E}_i^T(t)P_{i1}\bar{E}_i(t) + \tilde{E}_i^T(t)P_{i2}\tilde{E}_i(t)$.

Substituting $P_i = \begin{bmatrix} P_{i1} & O \\ O & P_{i2} \end{bmatrix}$ and $Q_i = \begin{bmatrix} Q_{i1} & O \\ O & Q_{i2} \end{bmatrix}$ into (25), we get:

$$
\begin{bmatrix} Q_{i1} & O \\ O & Q_{i2} \end{bmatrix} + (\begin{bmatrix} P_{i1} & O \\ O & P_{i2} \end{bmatrix}\begin{bmatrix} \bar{A}_i + \bar{B}_i\bar{K}_i & -\bar{B}_i\bar{K}_i \\ O & \bar{A}_i + L_i\bar{C}_i \end{bmatrix}) + (\begin{bmatrix} P_{i1} & O \\ O & P_{i2} \end{bmatrix}\begin{bmatrix} \bar{A}_i + \bar{B}_i\bar{K}_i & -\bar{B}_i\bar{K}_i \\ O & \bar{A}_i + L_i\bar{C}_i \end{bmatrix})^T
$$
$$
+ \begin{bmatrix} \bar{K}_i^T R_i \bar{K}_i & -\bar{K}_i^T R_i \bar{K}_i \\ -\bar{K}_i^T R_i \bar{K}_i & \bar{K}_i^T R \bar{K}_i \end{bmatrix} + \frac{1}{\rho_i^2}\begin{bmatrix} P_{i1}P_{i1} & O \\ O & P_{i2}P_{i2} \end{bmatrix} = \begin{bmatrix} M_1 & -P_{i1}\bar{B}_i\bar{K}_i - \bar{K}_i^T R_i \bar{K}_i \\ * & M_2 \end{bmatrix} \leq 0
$$
(29)

where $M_1 = Q_{i1} + (P_{i1}(\bar{A}_i + \bar{B}_i\bar{K}_i)) + (P_{i1}(\bar{A}_i + \bar{B}_i\bar{K}_i))^T + \bar{K}_i^T R_i \bar{K}_i + \frac{1}{\rho_i^2}P_{i1}P_{i1}$,
$M_2 = Q_{i2} + (P_{i2}(\bar{A}_i + L_i\bar{C}_i)) + (P_{i2}(\bar{A}_i + L_i\bar{C}_i))^T + \bar{K}_i^T R_i \bar{K}_i + \frac{1}{\rho_i^2}P_{i2}P_{i2}$.

By the fact that $\begin{bmatrix} M_1 & -P_{i1}\bar{B}_i\bar{K}_i - \bar{K}_i^T R_i \bar{K}_i \\ * & M_2 \end{bmatrix} \leq 0 \Rightarrow M_1 \leq 0, M_2 \leq 0$, the inequality $M_1 \leq 0$ is used to find $P_{i1}, \bar{K}_i$. We premultiply and postmultiply $M_1 \leq 0$ by $W_{i1} = P_{i1}^{-1}$ and applying Lemma 2, we obtain the following LMI

$$
\begin{bmatrix} \Delta_{11} & W_{i1} Q_{i1}^{1/2} & Y_{i1}^T \\ * & -I & O \\ * & * & -R_i^{-1} \end{bmatrix} \leq 0
$$
(30)

where $\Delta_{11} = \bar{A}_i W_{i1} + \bar{B}_i Y_{i1} + (\bar{A}_i W_{i1} + \bar{B}_i Y_{i1})^T + \frac{1}{\rho_i^2}I$, and $Y_{i1} = \bar{K}_i W_{i1}$. By solving the LMI in (30), we can obtain W_{i1}, Y_{i1} and therefore the PID controller gain $\bar{K}_i = Y_{i1}W_{i1}^{-1}$.

Step 2: By substituting $P_{i1} = W_{i1}^{-1}$ and $\bar{K}_i = Y_{i1}W_{i1}^{-1}$, as obtained in *Step 1*, into (29) and applying Lemma 2, we derive

$$
\begin{bmatrix} M_1 & -P_{i1}\bar{B}_i\bar{K}_i - \bar{K}_i^T R_i \bar{K}_i & O \\ * & \Delta_{22} & P_{i2} \\ * & * & -\rho_i^2 I \end{bmatrix} \leq 0
$$
(31)

where $\Delta_{22} = Q_{i2} + P_{i2}\bar{A}_i + Y_{i2}\bar{C}_i + (P_{i2}\bar{A}_i + Y_{i2}\bar{C}_i)^T + \bar{K}_i^T R_i \bar{K}_i$, and $Y_{i2} = P_{i2}L_i$. By solving the LMI in (31) using the LMI TOOLBOX in MATLAB, the values of P_{i2}, Y_{i2} can be determined, from which the observer gain L_i is computed as $P_{i2}^{-1}Y_{i2}$.

However, due to the integral action of the controller, actuator saturation is always a concern in this PID control design. This is because the control law is inevitably limited and restricted by the physical saturation of the actuator in the practical application of LEO satellites. The PID control law of the ith LEO satellite $u_{pid,i}(t) = [u_{i1}(t), u_{i2}(t), u_{i3}(t), u_{i4}(t), u_{i5}(t), u_{i6}(t)]^T$ differs in operational ranges. As a result, applying a distinctive constraint on each physical input is necessary. Suppose that $\hat{\bar{E}}_i(t)$ is restricted to stay in an invariant ellipsoid $\varepsilon_r = \{\hat{\bar{E}}_i(t) \in \mathbb{R}^{(18+(k_a+1)n+(k_s+1)m)} | \hat{\bar{E}}_i^T(t) W_{i1}^{-1} \hat{\bar{E}}_i(t) \le 1\}$ for $t \ge 0$, and if $v_{ip}^2 W_{i1}^{-1} \ge (T_p \bar{K}_i)^T T_p \bar{K}_i$ for actuator saturation constraint $v_{ip} \in \mathbb{R}^+$, then we can obtain[1]:

$$
\begin{aligned}
\max_{t \ge 0} \ & |u_{ip}(t)| \\
= \max_{t \ge 0} \ & \|u_{ip}(t)\|_2 \\
= \max_{t \ge 0} \ & \|T_p u_{pid,i}(t)\|_2 \\
\le \max_{t \ge 0} \ & \|T_p \bar{K}_i \hat{\bar{E}}_i(t)\|_2 \\
\le \max_{\bar{E}_i \in \varepsilon_r} \ & \|T_p \bar{K}_i \hat{\bar{E}}_i(t)\|_2 \\
\le \max_{\bar{E}_i \in \varepsilon_r} \ & \|v_{ip} W_{i1}^{-\frac{1}{2}} \hat{\bar{E}}_i(t)\|_2 \\
= \max_{\bar{E}_i \in \varepsilon_r} \ & \sqrt{v_{ip}^2 \hat{\bar{E}}_i^T(t) W_{i1}^{-1} \hat{\bar{E}}_i(t)} \\
\le \ & v_{ip} \ for \ p = 1, ..., 6, \quad i = 1, ..., N
\end{aligned}
\tag{32}
$$

where $T_1 = diag(1, 0, 0, 0, 0, 0)$, $T_2 = diag(0, 1, 0, 0, 0, 0)$, $T_3 = diag(0, 0, 1, 0, 0, 0)$, $T_4 = diag(0, 0, 0, 1, 0, 0)$, $T_5 = diag(0, 0, 0, 0, 1, 0)$, $T_6 = diag(0, 0, 0, 0, 0, 1)$

That is, if $v_{ip}^2 W_{i1}^{-1} \ge \bar{K}_i^T(t) \bar{K}_i(t)$ or $v_{ip}^2 W_{i1} \ge (\bar{K}_i W_{i1})^T \bar{K}_i W_{i1} = Y_{i1}^T Y_{i1}$ holds , then $\max_{t \ge 0} |u_{ip}(t)| \le v_{ip}$ for $t \ge 0$, $p = 1, ..., 6$; in other words, $u_{ip}(t)$ is under the actuator saturation v_{ip}. Therefore, by Schur complement in Lemma 2, the above actuator saturation constraints are equivalent to the following LMIs:

$$
\begin{bmatrix} v_{ip}^2 W_{i1} & Y_{i1}^T T_p^T \\ * & I \end{bmatrix} \ge 0, \ for \ p = 1, ..., 6
\tag{33}
$$

If the optimal robust H_∞ decentralized fault-tolerant observer-based PID team formation tracking control strategy in (22) with the consideration of actuator saturation v_{ip} in (32) and (33) is employed for the augmented tracking and estimation error system in (21) of each satellite in the large-scale team formation of LEO satellites, we need to solve the following LMIs-constrained optimization problem for each LEO satellite in the team formation:

$$
\begin{aligned}
\rho_i^{*2} = \min_{Y_{i1}, Y_{i2}, W_{i1} > 0, P_{i2} > 0} & \rho_i^2 \\
s.t.((30)), ((31)), ((33)) &
\end{aligned}
\tag{34}
$$

Remark 3 (i) The actuator saturation constraints in (32) are based on $\hat{\bar{E}}_i^T(t) W_{i1}^{-1} \hat{\bar{E}}_i(t) \le 1$, meaning that $\hat{\bar{E}}_i(t)$ remains within an invariant ellipsoid and finite. As a result, the stability of the proposed H_∞ fault-tolerant decentralized observer-based PID team formation control strategy of (22), as presented in Theorem 1, is guaranteed. (ii) Applying the above optimization technique to addressing LMI problems in (33) frequently yields a conservative solution, potentially imposing excessive restrictions (i.e., inequalities) on the calculated input gain in (32), consequently compromising performance. To fully harness the control potential, it is advisable to set the constrained value v_{ip} at a level higher than the actual one in (33). (iii) The design complexity in (34) mainly lies in how to solve three LMIs in (30), (31) and (33), which is mainly based on Newton searching algorithm to search $P_{i2} > 0$ in (31) and $W_{i1} > 0$ in (30) and (33). The computational complexity is $O(l(l+1))$, where l is the dimension of P_{i2} or W_{i1}[38]. Therefore, the design complexity of solving the LMIs-constrained optimization problem in (34) is $O(3N(l+1)l)$, where N is the number of LEO satellites.

Remark 4 The optimal H_∞ decentralized observer-based PID team formation control design problem with actuator saturation constraint in (34) can be solved by decreasing ρ_i^2 until there exists no $W_{i1} > 0$ or $P_{i2} > 0$ to obtain the minimum ρ_i^{*2} with $Y_{i1}^*, Y_{i2}^*, W_{11}^* > 0$ and $P_i^* > 0$, which can be solved by MATLAB in Algorithm 1 using the LMI TOOLBOX. Therefore, the decentralized H_∞ fault-tolerant observer-based team formation PID control gain $\bar{K}_i^* = Y_{i1}^* W_{i1}^{*-1}$ and observer gain $L_i^* = p_{i2}^* Y_{i2}^*$ can be obtained in a single run of decreasing ρ_i^2 in (34) with the help of LMI TOOLBOX in MATLAB, unlike the conventional PID control design algorithms, which need a very complicated parameter tuning.

Based on the above analyses, the main challenge of implementing this H_∞ fault-tolerant decentralized observer-based PID formation tracking control strategy is mainly divided into two steps: (i) Based on the solution $Y_{i1}^*, Y_{i2}^*, W_{i1}^*$ and P_{i2}^* of the LMIs-constrained optimization problem in (34) for PID control gain $\bar{K}_i^*$ and observer gain L_i^* of the Luenberger observer-based PID controller in (19), (ii) Based on the PID controller and target reference $r_i(t)$, it is easy to implement the reference-based feedforward linearization control law $u_i(t)$ in (4) for each LEO satellite in (3) of the team formation. The implementation of the decentralized observer-based PID team formation tracking control strategy of large-scale LEO satellites is shown in Figure 4.

Remark 5 The design complexity of the solution of the LMI-constrained optimization problem in (34) for ρ_i^{*2} with $Y_{i1}^*, Y_{i2}^*, W_{11}^* > 0$ and $P_i^* > 0$ to obtain observer gain $L_i^* = p_{i2}^{*-1} Y_{i2}^*$ and control gain $\bar{K}_i^* = Y_{i1}^* W_{i1}^{*-1}$ for the Luenberger observer-based PID controller in (19) mainly lies in solving LMIs in (30), (31) and (34).

The design procedure of the optimal decentralized H_∞ fault-tolerant observer-based PID team formation control design problem for each satellite in (3) is shown as follows:

1. Apply the feedforward control $u_i(t)$ in (4) for each LEO satellite in (3) to obtain the linearized tracking error dynamic system in (11) for each satellite.
2. Construct the smoothing signal models (14) and (16) for the actuator fault $f_{a,i}(t)$ and sensor fault $f_{s,i}(t)$, and embed these smoothing signal models into the linearized system (11) to get the augmented tracking error system of each satellite in (17).
3. Employ the observer-based fault-tolerant PID control tracking design in (19) to achieve the decentralized robust H_∞ fault-tolerant observer-based PID team formation control strategy in (22) with adequate weighting matrices Q_{i1}, Q_{i2} and R_i, actuator saturation v_{ip} in (33) and initial ρ_i.
4. Solve the LMI-constrained optimization problem in (34) for $Y_{i1}^*, Y_{i2}^*, W_{i1}^* > 0$ and $P_{i2}^* > 0$ under the actuator saturation v_{ip} by the two-step design procedure to obtain the fault-tolerant PID control gain $\bar{K}_i^* = Y_{i1}^* W_{i1}^{*-1}$ and observer gain $L_i^* = P_{i2}^{*-1} Y_{i2}^*$ for fault-tolerant observer-based controller in (19) of each satellite.

For more practical application, the above design procedure can be designed in

---

Algorithm 1 *Optimal Robust Decentralized H_∞ Fault-Tolerant Observer-Based PID Team Formation Tracking Control Design for NCS of Large-Scale LEO Satellites*

Require: *Smooth signal model parameters a_j, b_l; weighting matrices $Q_{i1} \geq 0$, $Q_{i2} \geq 0$, $R_i > 0$; initial ρ_i°; decreasing step $\rho_{i,s}$; actuator saturation upper bound v_{ip};*
Ensure: *Optimal PID control gain $\bar{K}_i^*$, optimal observer gain L_i^* in (19) and optimal attenuation level ρ_i^**
  1: *while $i \leq N$ do*
  2:    *if Assumption 2 holds **then***
  3:       *Solve the BMI problem in (25) with two-step LMIs;*
  4:       *Step 1:*
  5:       *Solve LMIs in (30) and (33) to get Y_{i1}, W_{i1} and control gain $\bar{K}_i = Y_i W_{i1}^{-1}$;*
  6:       *if $P_{i1} > 0$ and $M_1 < 0$ in (29) **then***
  7:          *Step 2:*
  8:          *Substituting W_{i1}, Y_{i1} and $\bar{K}_i$ into (31);*
  9:          *Solve the LMIs problem (31) to get Y_{i2}, P_{i2} and $L_i = P_{i2}^{-1} Y_{i2}$;*
 10:          *if $P_{i2} > 0$ and (31) holds **then***
 11:             *Update optimal solution*
 12:                *$\bar{K}_i^* \leftarrow \bar{K}_i$; $L_i^* \leftarrow L_i$; $\rho_i^* \leftarrow \rho_i^\circ$;*

13:     $\rho_i^{\circ} \leftarrow \rho_i^{\circ} - \rho_{i,s}$
14:         *end if*
15:     *else*
16:         *Can't solve LMIs problem, redesign;*
17:         *end if*
18:     *else*
19:         *Smooth signal models are unobservable, redesign* a_j *in* (13) *and* b_l *in* (15);
20:     *end if*
21: *end while*

---

4. SIMULATION AND COMPARISON

In the future 6G wireless communication era, large-scale satellite constellations will be developed using low-orbit satellites. In the limited space of LEO, the intersection of satellite orbits seems unavoidable. In this simulation scenario, we consider not only the altitude and attitude of satellites within a single orbit but also the team formation involving the crossing of four different satellite orbits at the same altitude. By implementing appropriate orbit planning and maintaining precise altitude and attitude control, these LEO satellites can not only be easily employed for coverage service tasks but also effectively prevent collision incidents.

4.1 Design specifications of the satellites system

Suppose 12 satellites in a team [Figure 5] are employed for a mission with four different orbits with an inclination of 50° and an altitude of 1,000 km. Each orbit has three followers to form an equilateral angle and one virtual leader in the centroid of the triangle, as shown in Figure 6. In the relative dynamic of each LEO satellite in (1), the earth gravitational parameter $u_e = 398,600$ km^3/s^2, the orbital velocity $v_{ECI,z_i} = \sqrt{\frac{u_e}{R_o}}$, where $R_o = 7,371$ km from the virtual leader to the earth[35]. The other parameters in (1) are given as follows: $m_i = 150$ kg, the inertia matrix $J_k^i = diag(35, 20, 16)$ kg/m^2, $k = 1, 2, 3$, $i = 1, \ldots 12$[36]. Moreover, the sampling period $h = 0.001$ s in this simulation.

Due to the corruption effect of malicious attack signals via two wireless network channels [Figure 4], two fifth-order ($k_a = k_b = 4$) smoothing models in (14) and in (16) are used to model actuator and sensor fault signals, respectively. In this simulation example, the equivalent actuator fault signal $f_{a,i}(t)$ and sensor fault signal $f_{s,i}(t)$ on the 12th satellite system are shown in Figure 7 and Figure 8, respectively, and the extrapolation parameters are specified as $a_0 = 0.8$, $a_1 = 0.1$, $a_2 = 0.06$, $a_3 = 0.03$, $a_4 = 0.01$, $b_0 = 0.9$, $b_1 = 0.06$, $b_2 = 0.02$, $b_3 = 0.01$ and $b_4 = 0.01$ to satisfy the observability condition in (18).

Besides, the effect of the following environmental disturbances in each satellite orbit such as solar radiation pressure, earth flattening, and aerodynamic drag in (1), (2),[21], [36] must be considered in the design procedure:

$$d_i(t) = [10^{-7}(38.9 \sin^2(v_{ECI,z_i}t) + 7.88 \cos(v_{ECI,z_i}t) \sin(v_{ECI,z_i}t) - 88.8),$$
$$10^{-8}(-131 \sin(2v_{ECI,z_i}t) + 833 \cos^2(v_{ECI,z_i}t) - 4.96 \cos(v_{ECI,z_i}t) - 13.5),$$
$$-6.28 \times 10^{-6} \sin(v_{ECI,z_i}t), \ 5 \times 10^{-3} \sin(0.1t), \ 5 \times 10^{-3} \cos(0.1t), \ 5 \times 10^{-3} \sin(0.15t)]^T$$
$$\text{for } i = 1, ..., 12. \tag{35}$$

The CCI can manifest between satellites. Based on the characteristics of CCI, its potency correlates with the separation distance between the two transmitters. In essence, when two satellites are in close proximity, the CCI's influence becomes more pronounced. Consequently, CCI predominantly emerges between two neighboring satellites within the formation consortium. Within this simulation, the coupling terms are employed to depict the impact of CCI on the satellite system as follows[40]:

$$c_{ij}(t) = [0.01\dot{x}_i(t)\dot{x}_j(t - 0.1), 0.01\dot{y}_i(t)\dot{y}_j(t - 0.1), 0.01\dot{z}_i(t)\dot{z}_j(t - 0.1)$$
$$, 0.01\dot{\theta}_1^i(t)\dot{\theta}_1^j(t - 0.1), 0.01\dot{\theta}_2^i(t)\dot{\theta}_2^j(t - 0.1), 0.01\dot{\theta}_3^i(t)\dot{\theta}_3^j(t - 0.1)]^T$$
$$\text{for } i = 1, ..., 12, j \neq i, j = 1, ..., 12. \tag{36}$$

where the velocity and angle velocity of the jth satellite $\dot{x}_j, \dot{y}_j, \dot{z}_j, \dot{\theta}_1^j, \dot{\theta}_2^j, \dot{\theta}_3^j$ are related to the CCI effect caused by the jth neighboring satellite on the ith satellite.
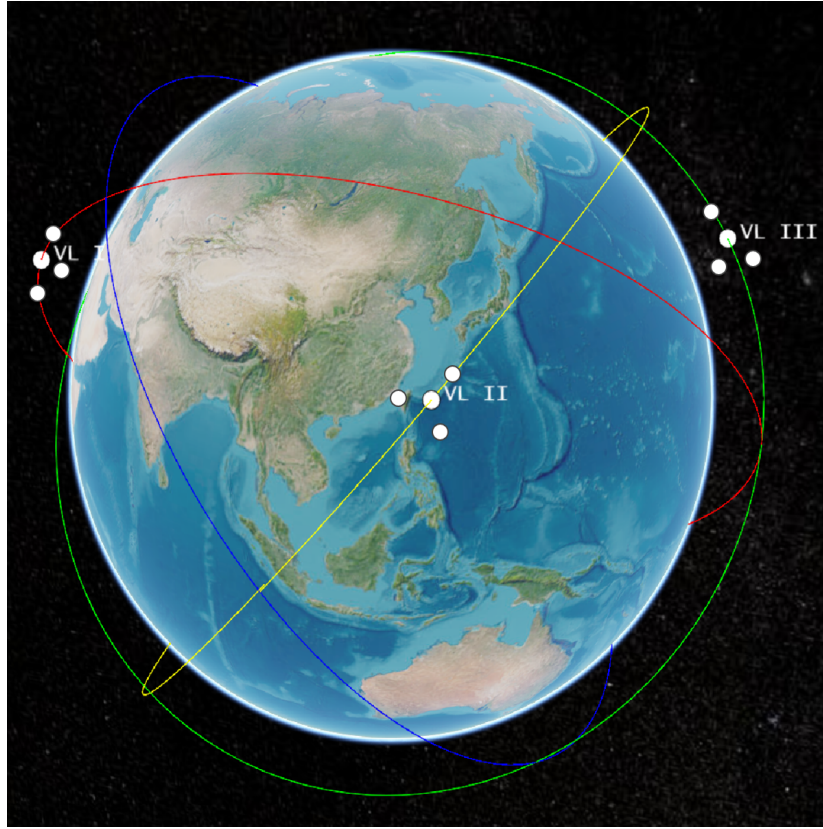
Figure 5. A team formation of 12 LEO satellites with coverage service in four crossing orbits (the fourth virtual leader is on another hemisphere).

For the decentralized H$_\infty$ fault-tolerant observer-based PID team formation Control design strategy of LEO satellites in (22), the weighting matrices Q_{i1}, Q_{i2}, R_i, the initial ρ_i°, the decreasing step $\rho_{i,s}$ and the actuator saturation upper bound v_{ip} are assigned to execute a task as follows:

$$Q_{i1} = diag(\Xi_1, \Xi_2, \Xi_3), Q_{i2} = diag(\Xi_4, \Xi_5, \Xi_6), R_i = 10^{-6} \times I_6, \rho_i^\circ = 100, \rho_{i,s} = 0.01, \tag{37}$$
$$v_{i1}, v_{i2}, v_{i3} = 3500, \ v_{i4} = 1600, v_{i5} = 1500, v_{i6} = 1400, t_f = 5400 sec$$

where $\Xi_1 = diag(0.01, 0.01, 0.01, 0.01, 0.01, 0.01, 1, 1, 1, 10, 10, 10, 0.1, 0.1, 0.1, 0.1, 0.1, 0.1), \Xi_2 = O_{30}, \Xi_3 = O_{30}$,
$\Xi_4 = diag(0.12, 0.12, 0.12, 0.12, 0.12, 0.12, 12, 12, 12, 120, 120, 120, 1.2, 1.2, 1.2, 1.2, 1.2, 1.2)$,
$\Xi_5 = 0.3 \times diag(0.1, 0.01) \otimes I_{15}$ and $\Xi_6 = 60 \times diag(0.1, 0.01) \otimes I_{15}$

In this simulation example, the orbits of the virtual leaders are shown in Figure 5. The orbital elements are given as follows:

$$semi-major\ axis = 7371km, \quad eccentricity = 0,$$
$$inclination = 50°, \quad true\ anomaly = 0, \quad argument\ of\ periapsis = 0 \tag{38}$$
$$longitude\ of\ the\ ascending\ node = 0°, 90°, 180°, 270°$$

The followers of each virtual leader are shown in Figure 6, with three followers forming an equilateral triangle in which the length of three sides are all 50km and the virtual leader lies in the centroid of the triangle. In the satellite attitude for this task of coverage service, the desired attitude reference trajectories are specified for 12 satellites as
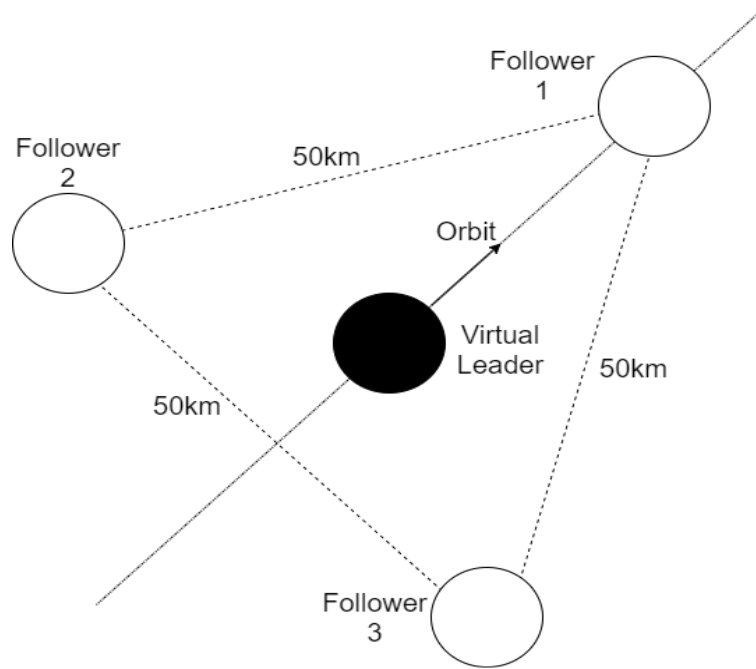
Figure 6. A virtual leader in satellite formation system.

Table 1. The reference trajectories of 12 satellites (i.e., the formation shape $(\bar{r}_1^T(t), ...\bar{r}_i^T(t), ...\bar{r}_{12}^T(t))^T)$ of a team formation for the mission of coverage service in four orbits in simulation, where $\theta_{r_1}^i(t)$, $\theta_{r_2}^i(t)$ and $\theta_{r_3}^i(t)$ are given in (39)

Orbit	Satellite	The reference $\bar{r}_i(t)$
Orbit I	Satellite1	$\bar{r}_1(t) = [28.8675, 0, 0, \theta_{r_1}^1, \theta_{r_2}^1, \theta_{r_3}^1, 0, 0, 0, \dot{\theta}_{r_1}^1, \dot{\theta}_{r_2}^1, \dot{\theta}_{r_3}^1]^T$
Orbit I	Satellite2	$\bar{r}_2(t) = [-14.4338, 0, 25, \theta_{r_1}^2, \theta_{r_2}^2, \theta_{r_3}^2, 0, 0, 0, \dot{\theta}_{r_1}^2, \dot{\theta}_{r_2}^2, \dot{\theta}_{r_3}^2]^T$
Orbit I	Satellite3	$\bar{r}_3(t) = [-14.4338, 0, -25, \theta_{r_1}^3, \theta_{r_2}^3, \theta_{r_3}^3, 0, 0, 0, \dot{\theta}_{r_1}^3, \dot{\theta}_{r_2}^3, \dot{\theta}_{r_3}^3]^T$
Orbit II	Satellite4	$\bar{r}_4(t) = [28.8675, 0, 0, \theta_{r_1}^4, \theta_{r_2}^4, \theta_{r_3}^4, 0, 0, 0, \dot{\theta}_{r_1}^4, \dot{\theta}_{r_2}^4, \dot{\theta}_{r_3}^4]^T$
Orbit II	Satellite5	$\bar{r}_5(t) = [-14.4338, 0, 25, \theta_{r_1}^5, \theta_{r_2}^5, \theta_{r_3}^5, 0, 0, 0, \dot{\theta}_{r_1}^5, \dot{\theta}_{r_2}^5, \dot{\theta}_{r_3}^5]^T$
Orbit II	Satellite6	$\bar{r}_6(t) = [-14.4338, 0, -25, \theta_{r_1}^6, \theta_{r_2}^6, \theta_{r_3}^6, 0, 0, 0, \dot{\theta}_{r_1}^6, \dot{\theta}_{r_2}^6, \dot{\theta}_{r_3}^6]^T$
Orbit III	Satellite7	$\bar{r}_7(t) = [28.8675, 0, 0, \theta_{r_1}^7, \theta_{r_2}^7, \theta_{r_3}^7, 0, 0, 0, \dot{\theta}_{r_1}^7, \dot{\theta}_{r_2}^7, \dot{\theta}_{r_3}^7]^T$
Orbit III	Satellite8	$\bar{r}_8(t) = [-14.4338, 0, 25, \theta_{r_1}^8, \theta_{r_2}^8, \theta_{r_3}^8, 0, 0, 0, \dot{\theta}_{r_1}^8, \dot{\theta}_{r_2}^8, \dot{\theta}_{r_3}^8]^T$
Orbit III	Satellite9	$\bar{r}_9(t) = [-14.4338, 0, -25, \theta_{r_1}^9, \theta_{r_2}^9, \theta_{r_3}^9, 0, 0, 0, \dot{\theta}_{r_1}^9, \dot{\theta}_{r_2}^9, \dot{\theta}_{r_3}^9]^T$
Orbit IV	Satellite10	$\bar{r}_{10}(t) = [28.8675, 0, 0, \theta_{r_1}^{10}, \theta_{r_2}^{10}, \theta_{r_3}^{10}, 0, 0, 0, \dot{\theta}_{r_1}^{10}, \dot{\theta}_{r_2}^{10}, \dot{\theta}_{r_3}^{10}]^T$
Orbit IV	Satellite11	$\bar{r}_{11}(t) = [-14.4338, 0, 25, \theta_{r_1}^{11}, \theta_{r_2}^{11}, \theta_{r_3}^{11}, 0, 0, 0, \dot{\theta}_{r_1}^{11}, \dot{\theta}_{r_2}^{11}, \dot{\theta}_{r_3}^{11}]^T$
Orbit IV	Satellite12	$\bar{r}_{12}(t) = [-14.4338, 0, -25, \theta_{r_1}^{12}, \theta_{r_2}^{12}, \theta_{r_3}^{12}, 0, 0, 0, \dot{\theta}_{r_1}^{12}, \dot{\theta}_{r_2}^{12}, \dot{\theta}_{r_3}^{12}]^T$

follows[41]:

$$\theta_{r_1}^i(t) = \begin{cases} \frac{2\pi t}{t_f}, & \text{for } t < \frac{t_f}{4} \\ \pi - \frac{2\pi t}{t_f}, & \text{for } \frac{t_f}{4} \le t < \frac{t_f}{2} \\ -\pi + \frac{2\pi t}{t_f}, & \text{for } \frac{t_f}{2} \le t < \frac{3t_f}{4} \\ 2\pi - \frac{2\pi t}{t_f}, & \text{for } \frac{3t_f}{4} \le t < t_f \end{cases} \quad \theta_{r_2}^i(t) = 0, \quad \theta_{r_3}^i(t) = \begin{cases} \frac{2\pi t}{t_f}, & \text{for } t < \frac{t_f}{4} \\ \pi - \frac{2\pi t}{t_f}, & \text{for } \frac{t_f}{4} \le t < \frac{t_f}{2} \\ -\pi + \frac{2\pi t}{t_f}, & \text{for } \frac{t_f}{2} \le t < \frac{3t_f}{4} \\ 2\pi - \frac{2\pi t}{t_f}, & \text{for } \frac{3t_f}{4} \le t < t_f \end{cases} \quad i = 1, 2, ..., 12$$

$$(39)$$

According to the above desired reference trajectory of each satellite, based on the desired target reference trajectory $r_i(t)$ of $q_i(t)$ in (4), we can get the reference trajectory $\bar{r}_i(t) = [r_i^T(t), \dot{r}_i^T(t)]^T$ for the trajectory $\bar{q}_i(t) = [q_i^T(t), \dot{q}_i^T(t)]^T$ of the ith satellite to track. The reference state $\bar{r}_i(t)$ of each satellite in the team (i.e., the formation shape $(\bar{r}_1^T(t), ...\bar{r}_i^T(t), ...\bar{r}_{12}^T(t))^T$ of 12 satellites) are shown in Table 1, and the initial states $\bar{q}_i(0)$ of each satellite are given in Table 2.

Table 2. The initial states of 12 satellites in team formation

Orbit	Satellite	The initial conditions $\bar{q}_i(t)$
Orbit I	Satellite1	$\bar{q}_1(0) = [25.1531, 1.2689, 2.0105, -0.4712, 0.2357, -0.1293, 0, 0, 0, 0, 0, 0]^T$
Orbit I	Satellite2	$\bar{q}_2(0) = [-10.0484, -2.2541, 26.0231, -0.2479, -0.3135, -0.5013, 0, 0, 0, 0, 0, 0]^T$
Orbit I	Satellite3	$\bar{q}_3(0) = [-12.5514, 3.0215, -25.5566, 0.3326, 0.2357, 0.0807, 0, 0, 0, 0, 0, 0]^T$
Orbit II	Satellite4	$\bar{q}_4(0) = [30.8913, -1.2643, 2.1234, -0.1268, 0.4411, 0.2266, 0, 0, 0, 0, 0, 0]^T$
Orbit II	Satellite5	$\bar{q}_5(0) = [-11.2922, 0.9527, 26.7523, 0.3331, -0.2748, -0.1056, 0, 0, 0, 0, 0, 0]^T$
Orbit II	Satellite6	$\bar{q}_6(0) = [-17.0031, -3.0274, -27.0018, 0.4090, -0.0156, 0.2348, 0, 0, 0, 0, 0, 0]^T$
Orbit III	Satellite7	$\bar{q}_7(0) = [29.9869, -4.0002, -3.6201, 0.3755, -0.1479, -0.0386, 0, 0, 0, 0, 0, 0]^T$
Orbit III	Satellite8	$\bar{q}_8(0) = [-18.4465, -3.2559, 27.0694, 0.4114, 0.2288, -0.1212, 0, 0, 0, 0, 0, 0]^T$
Orbit III	Satellite9	$\bar{q}_9(0) = [-17.2234, 2.0453, -22.8894, 0.3939, 0.1415, 0.3651, 0, 0, 0, 0, 0, 0]^T$
Orbit IV	Satellite10	$\bar{q}_{10}(0) = [25.6577, -2.7414, -2.6653, 0.3001, -0.1102, 0.2003, 0, 0, 0, 0, 0, 0]^T$
Orbit IV	Satellite11	$\bar{q}_{11}(0) = [-10.3051, 2.1556, 22.6096, 0.2513, 0.3209, -0.1889, 0, 0, 0, 0, 0, 0]^T$
Orbit IV	Satellite12	$\bar{q}_{12}(0) = [-13.1993, 1.8787, -22.9831, 0.2564, 0.4009, 0.1769, 0, 0, 0, 0, 0, 0]^T$
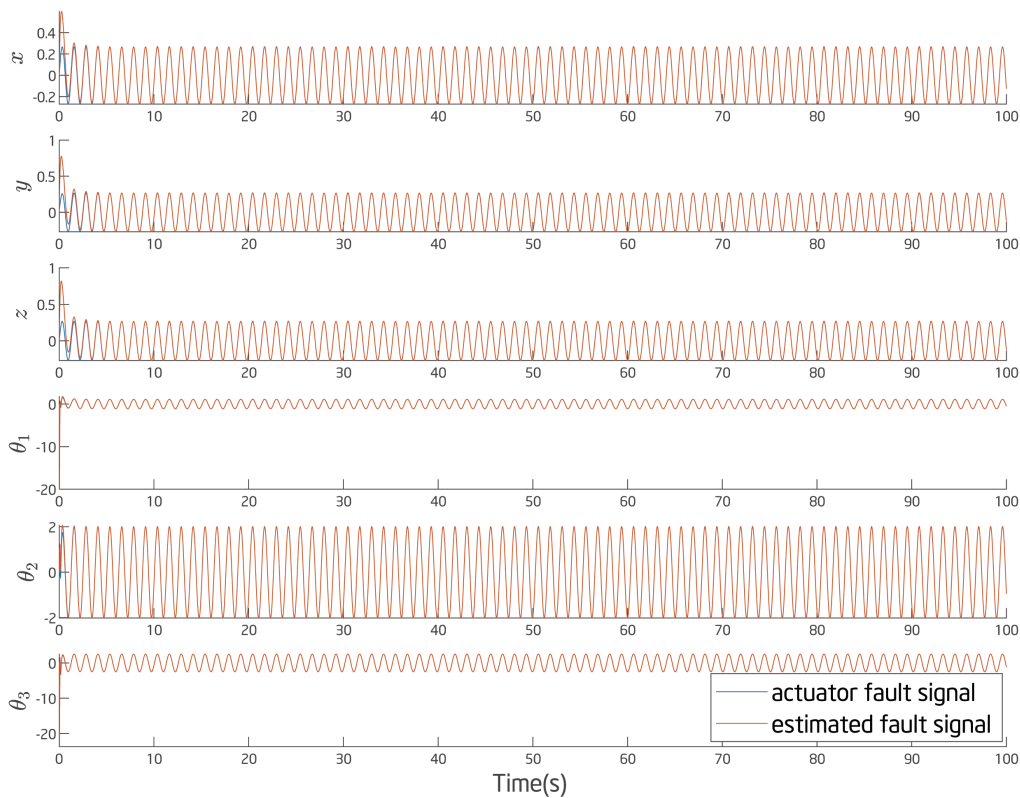
Figure 7. The equivalent fault signals of actuator $f_{a,12}(t)$ and their estimations of the 12th satellite NCS in the team.

4.2 Simulation and discussion

Using the above parameter settings and *Algorithm 1* to solve the LMI-constrained optimization problem in (34), the simulation results of the optimal robust H_∞ decentralized observer-based PID team formation control design for NCS of 12 satellites under external disturbance, CCI coupling and attack signals are obtained as follows.

Figure 7 shows the equivalent fault signals of actuator $f_{a,12}(t)$ in the 12th satellite and their estimations, and Figure 8 presents the fault signals of sensor $f_{s,12}(t)$ in the 12th satellite and their estimations. Due to a large initial state error, the initial estimation error of the Luenberger observer in (19) is also large. However, after the transient state of the Luenberger observer, the fault signals can be effectively estimated by the proposed optimal robust decentralized H_∞ observer-based fault-tolerant PID tracking control strategy in (22). Some fluctuations in the estimation of sensor faults $f_{s,12}(t)$ remain, which are caused by the sensor false signal in $y_i(t)$ that can directly influence the fault signal
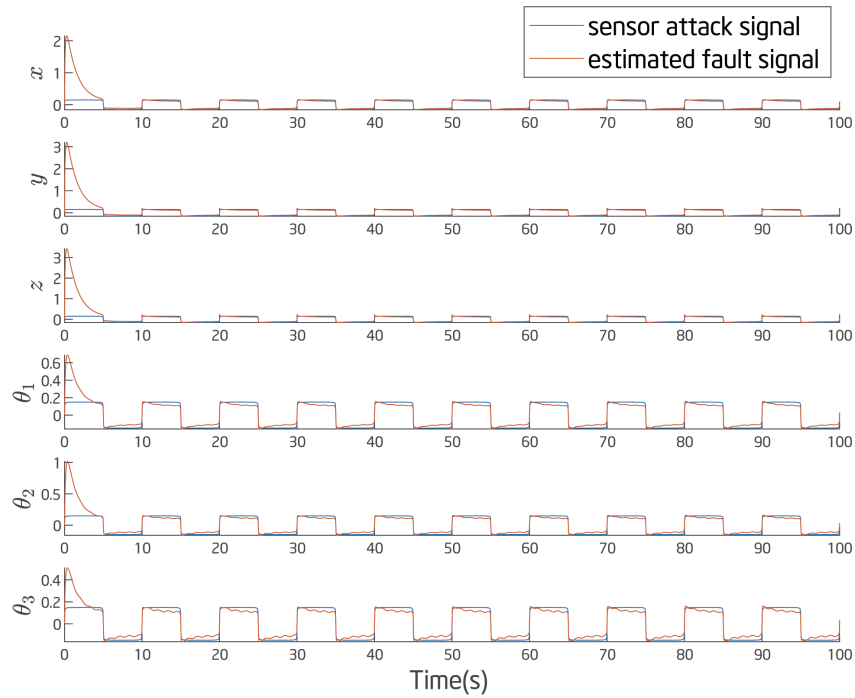
Figure 8. The equivalent fault signals of sensor $f_{s,12}(t)$ and their estimations of the 12th satellite NCS in the team.
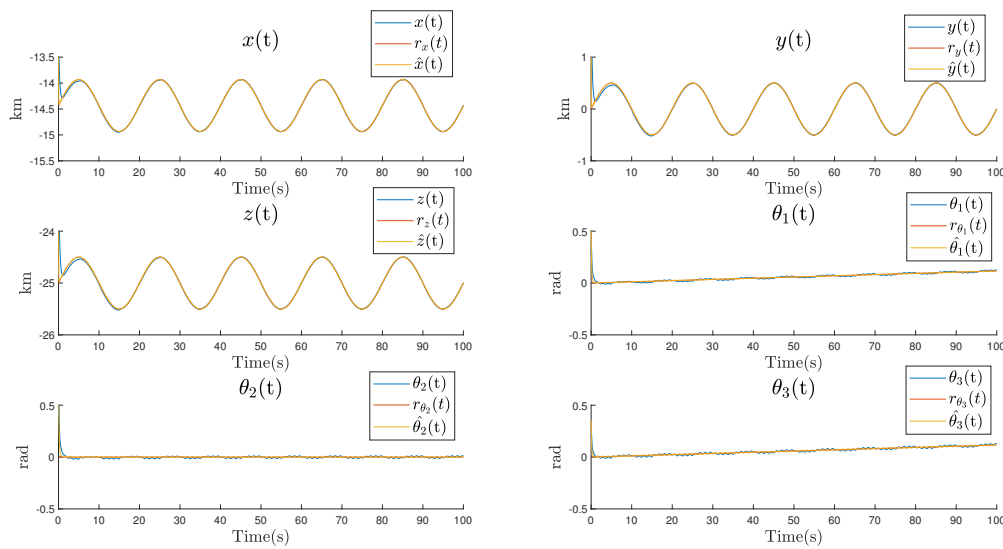
Figure 9. The relative altitude $(x_{12}(t), y_{12}(t), z_{12}(t))^T$ and attitude $(\theta_1^{12}(t), \theta_2^{12}(t), \theta_3^{12}(t))^T$ and their desired reference $(r_{x12}(t), r_{y12}(t), r_{z12}(t), r_{\theta_1,12}(t), r_{\theta_2,12}(t), r_{\theta_3,12}(t))^T$ and estimates $(\hat{x}_{12}(t), \hat{y}_{12}(t), \hat{z}_{12}(t), \hat{\theta}_1^{12}(t), \hat{\theta}_2^{12}(t), \hat{\theta}_3^{12}(t))^T$ of the 12th satellite of the team.

estimation in (19).

The tracking trajectories of the six states, estimated states and desired references of the 12th satellite are shown in Figure 9. It can be seen that the team formation tracking and estimation of satellites can reach and be maintained at the desired steady state under the influence of malicious attack signals, external disturbance and CCI coupling.

The relative distance and velocity of the first three follower satellites in orbit I of the team formation are given in Figure 10 and Figure 11, respectively. We can see that the relative distance of the satellite team formation can be kept with the desired triangle formation in Figure 6 in the steady state. Figure 12 and Figure 13 show the angle and
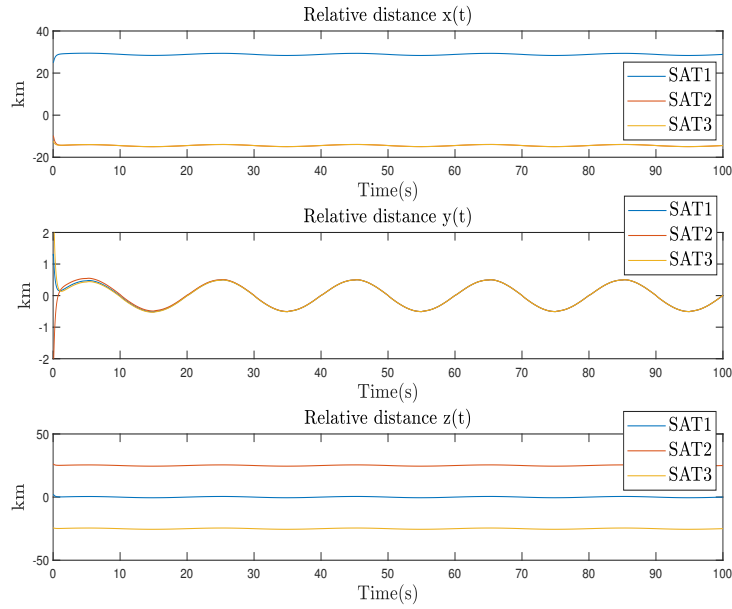
Figure 10. The formation performance of the relative distances of three satellites in orbit I.
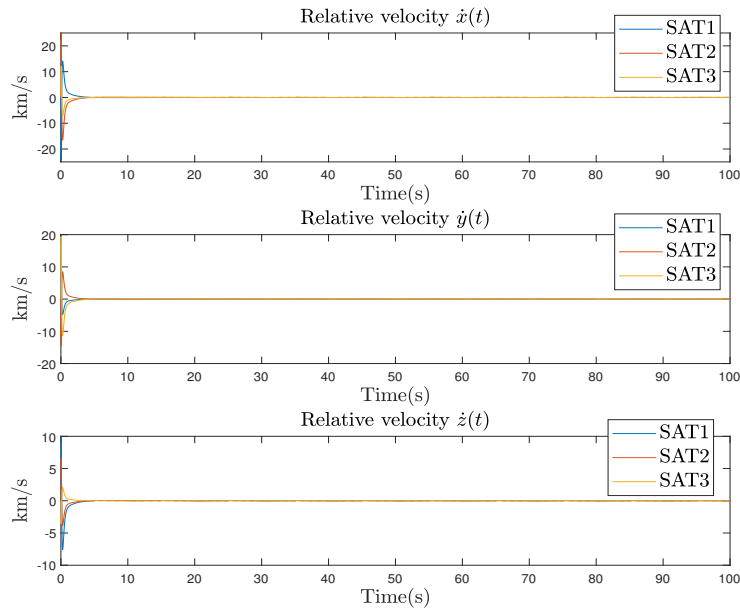
Figure 11. The performance of relative velocity tracking control of three satellites in orbit I.

angle velocity of the first three follower satellites in orbit I, respectively. It can be seen that the angle can be kept with the desired attitude we designed in (39) at the steady state. The relative distance and velocity of all 12 follower satellites in four orbits of the team formation are shown in Figure 14 and Figure 15, respectively. The tracking performance of angle and angle velocity (i.e., the attitude) of all 12 follower satellites in four orbits are shown in Figure 16 and 17, respectively.

The feedforward reference control inputs of the 12th satellite $u_{12}(t) = [u_{12x}(t), u_{12y}(t), u_{12z}(t),$
$u_{12\theta_1}(t), u_{12\theta_2}(t), u_{12\theta_3}(t)]^T$ in (3) are given in Figure 18. Due to the large initial trajectory error of each satellite, the beginning control inputs are large to push each satellite to its desired trajectory. Furthermore, the control inputs will be adjusted to compensate for the effect of fault signals to maintain the desired formation of each satellite when
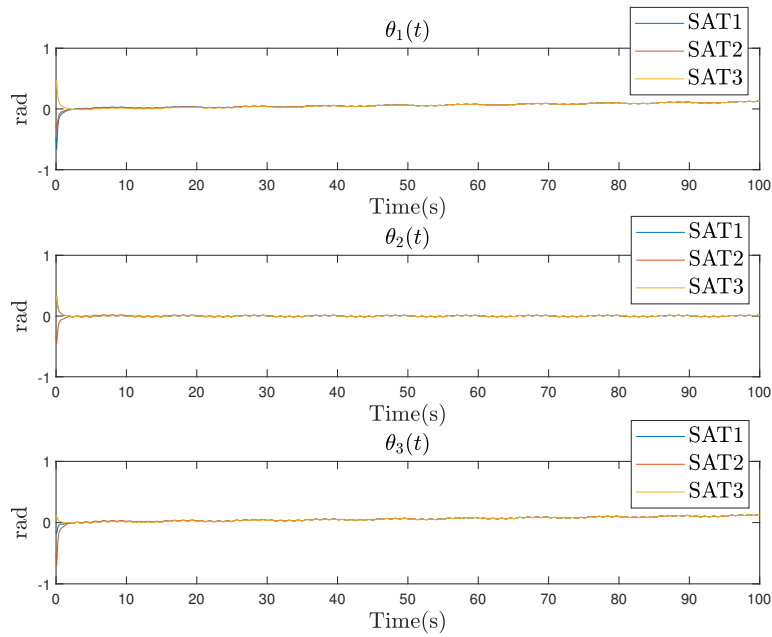
Figure 12. The performance of angular tracking control of three satellites in orbit I.
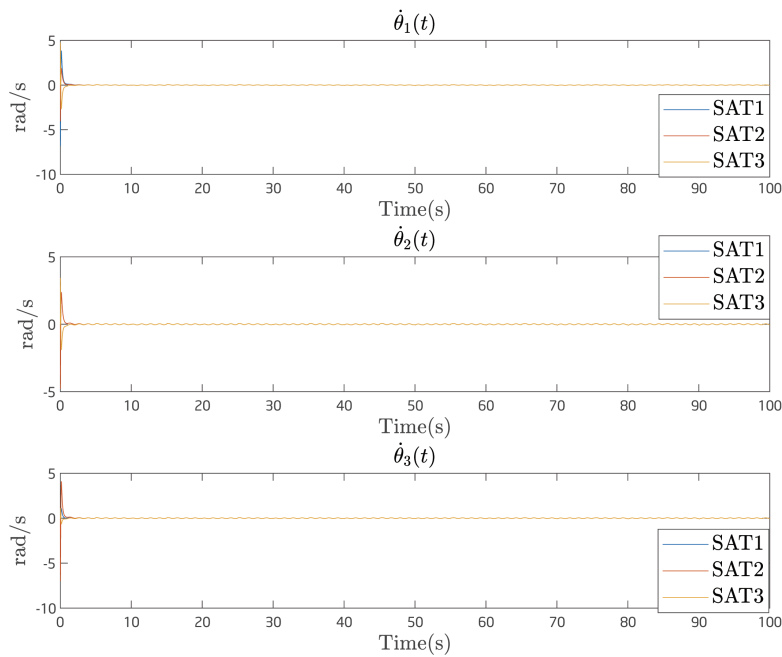
Figure 13. The performance of angle velocity tracking control of three satellites in orbit I.

these signals appear.

The average optimal $\rho_i^* = 34.13$, which is the average of 12 LMIs-constrained optimization in (34), i.e., $\frac{1}{12} \sum_{i=1}^{12} \rho_i^*$ obtained by the proposed *Algorithm 1*. The real H_∞ decentralized observer-based fault-tolerant PID team formation tracking control performance ρ_i^r, $i = 1, 2, ..., 12$ of 12 satellites in the NCS within $[0, 100s]$ by the computer
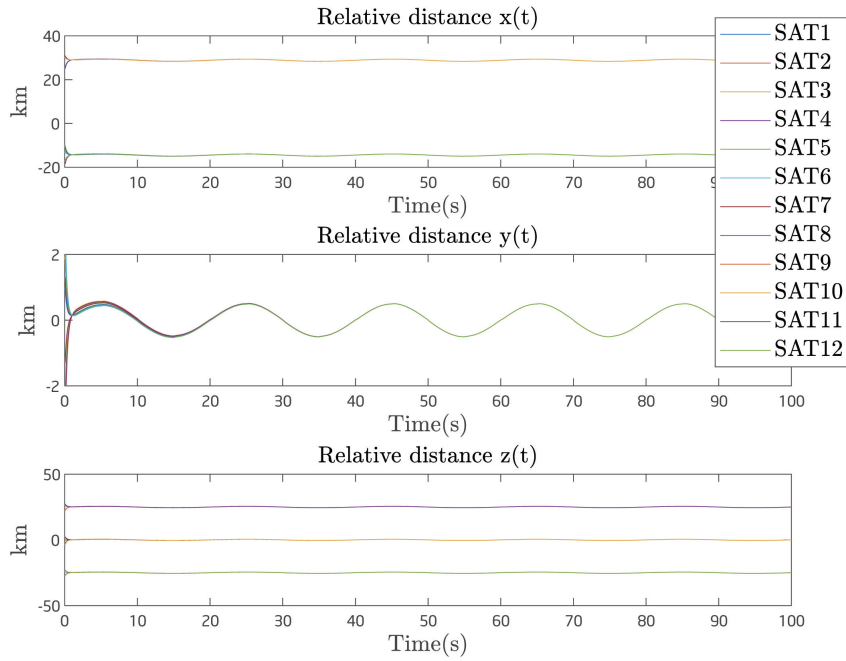
Figure 14. The relative distance tracking performance of all 12 satellites.
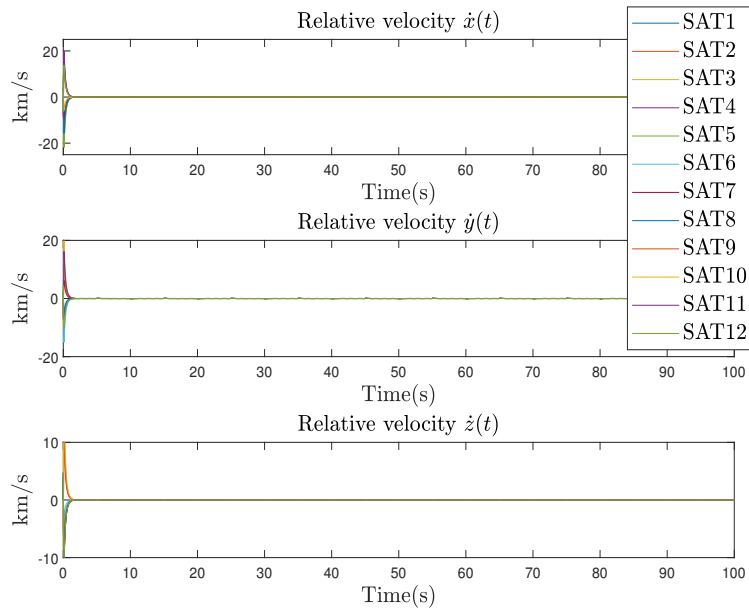
Figure 15. The relative velocity tracking performance of all 12 satellites.

simulation are calculated as follows:

$$\frac{\int_0^{100}(\bar{E}_i^T(t)Q_{i1}\bar{E}_i(t)+\tilde{E}_i^T(t)Q_{i2}\tilde{E}_i(t)+u_{pid,i}^T(t)R_i u_{pid,i}(t))dt-V(\tilde{S}_i(0))}{\int_0^{100}\tilde{v}_i^T(t)\tilde{v}_i(t)dt}=\rho_i^{r\,2} \quad i=1,2,...,12 \tag{40}$$

As shown in Table 3, the real average attenuation level of the proposed method is calculated as follows:

$$\frac{1}{12}\sum_{i=1}^{12}\rho_i^r = 1.2979 \tag{41}$$
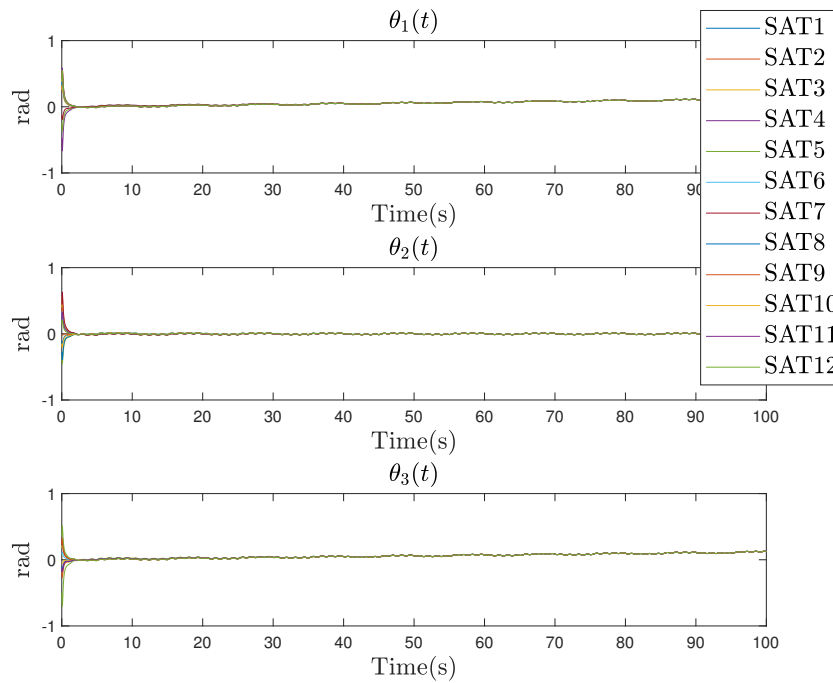
Figure 16. The angular tracking performance of all 12 satellites.

which is much less than the average optimal $\rho_i^* = 34.13$; i.e., the real result ρ_i^r in (40) of the proposed optimal H_∞ decentralized fault-tolerant observer-based PID team formation control scheme for NCS of 12 satellites is much better than the theoretical result ρ_i^* in (34). The reason for the conservative theoretical result is the use of inequalities in (26) and (27) for the proof of *Theorem 1* and the derivation of LMIs in (30) and (31) from Riccati-like inequalities in (25), the derivation of LMIs for the actuator saturation constraint in (32) and (33),and the solving process of the LMIs-constrained optimization problem in (34).Further ρ_i^* in (34) is based on the worst-case of all possible $\tilde{v}_i(t) \in L_2[0, 100]$ in (22) from the robust H_∞ observer PID team formation tracking control strategy. However, ρ_i^r in (40) and (41) is based on a real $\tilde{v}_i(t)$ and therefore is smaller than ρ_i^*.

According to the simulation results, we can validate that the proposed optimal robust H_∞ decentralized fault-tolerant observer-based PID team formation control strategy in (34) is effective for team formation of NCS of large-scale LEO satellites under the malicious attack signal, external disturbance, measurement noise, coupling effect and actuator saturation.

Remark 6 In practice, the communication time between the satellite and the ground station may be only a few minutes in one cycle. Therefore, our simulation time is considered to be 100 seconds, within which the trajectories of LEO satellites in the desired team formation could be estimated and tracked precisely by the proposed robust decentralized observer-based PID team formation control method.

4.3 Simulation comparison and discussion

In this subsection, for comparison, the decentralized robust H_∞ T-S fuzzy state feedback team formation control strategy in [24] is simulated for the satellite formation example with the same scenario. The tracking performance of altitudes and attitudes for the 1st satellite with fault signals by the proposed robust H_∞ fault-tolerant decentralized observer-based PID team formation control and the robust H_∞ T-S fuzzy decentralized state feedback control in [24] is given for comparison in Figure 19 and Figure 20, respectively. When fault signals appear, the H_∞ T-S fuzzy state feedback method in [24] will experience an offset. Then, the satellite cannot follow the desired trajectories because the method in [24] lacks the ability to handle FTC. Further, the decentralized H_∞ T-S fuzzy state feedback control method in [24] needs to interpolate 64 local linearized controllers by complicated fuzzy bases at every time instant, making it difficult to implement and perform in real-time at present. Obviously, the H_∞ T-S fuzzy state feedback team formation tracking control design in [24] is more complicated and its team formation tracking performance is
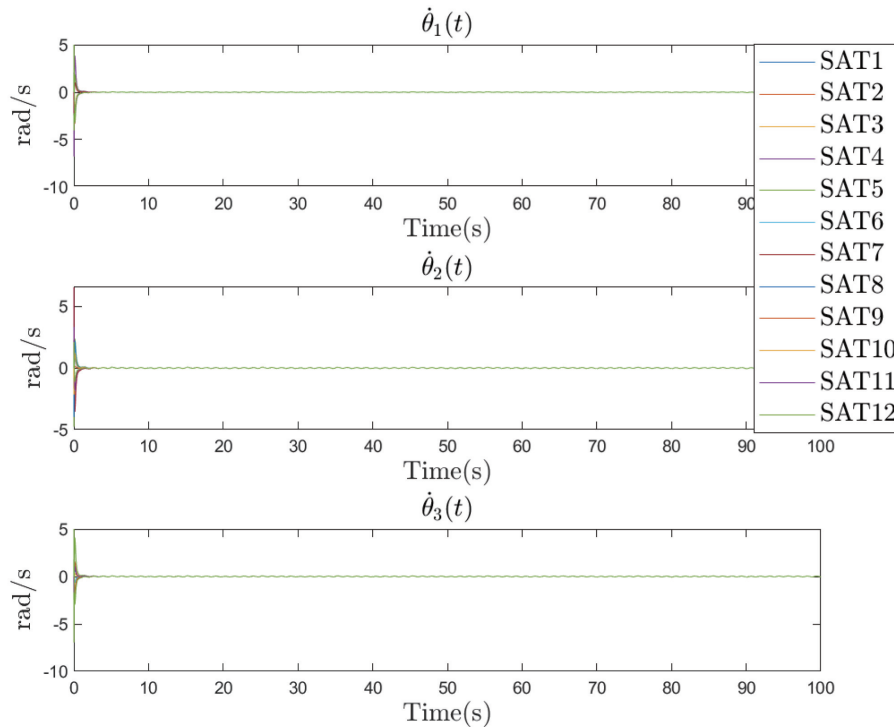
Figure 17. The angle velocity tracking performance of all 12 satellites.

Table 3. The real attenuation level ρ_i^r of 12 LEO satellites with a desired team formation for a coverage mission via the simulation within [0,100s]

Satellite	The real disturbance attenuation level $\rho_i^{r\,2}$
Satellite1	$\rho_1^{r\,2} = 1.3684^2$
Satellite2	$\rho_2^{r\,2} = 0.7051^2$
Satellite3	$\rho_3^{r\,2} = 1.2595^2$
Satellite4	$\rho_4^{r\,2} = 0.5763^2$
Satellite5	$\rho_5^{r\,2} = 1.2637^2$
Satellite6	$\rho_6^{r\,2} = 1.5155^2$
Satellite7	$\rho_7^{r\,2} = 2.0751^2$
Satellite8	$\rho_8^{r\,2} = 1.9365^2$
Satellite9	$\rho_9^{r\,2} = 0.9558^2$
Satellite10	$\rho_{10}^{r\,2} = 1.7294^2$
Satellite11	$\rho_{11}^{r\,2} = 1.5026^2$
Satellite12	$\rho_{12}^{r\,2} = 0.6871^2$

more conservative than the proposed method under actuator and sensor fault signals in the NCS of large-scale LEO satellites.

5. CONCLUSION

In this study, the robust H_∞ fault-tolerant decentralized observer-based PID team formation tracking control strategy is proposed for NCS of large-scale LEO satellites under the external disturbance, measurement noise, co-channel coupling and malicious attack signal. By using a novel reference-based feedforward linearization tracking control method, the design problem of nonlinear satellite team formation NCS becomes a linearized reference tracking control design problem with a corresponding actuator fault signal and measurement fault signal for each satellite. Then, smoothing models are embedded in a linearized team system to efficaciously estimate actuator and sensor fault signals for compensation to avoid their effect on the reference tracking estimation and PID tracking performance of each satellite. Moreover, by the proposed decentralized robust H_∞ fault-tolerant observer-based PID team formation control scheme, we can solve BMI by a two-step LMI design procedure via a simple LMIs-constrained optimization problem to achieve the optimal H_∞ robust fault-tolerant decentralized observer-based PID team formation NCS control of large-scale LEO satellites. A simulation example of team formation composed of 12 LEO satellites in
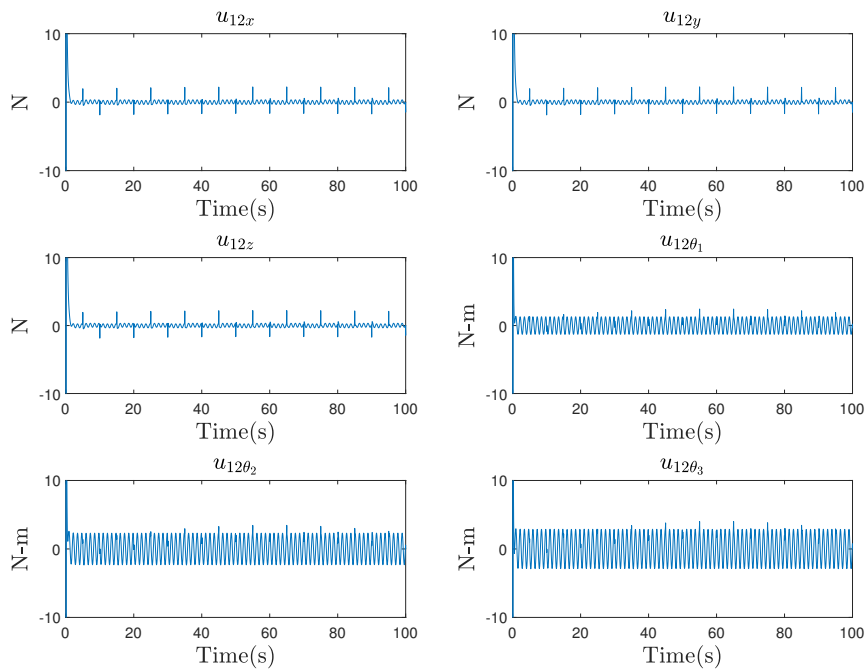
Figure 18. The control inputs $u_{12}(t) = [u_{12x}(t), u_{12y}(t), u_{12z}(t), u_{12\theta_1}(t), u_{12\theta_2}(t), u_{12\theta_3}(t)]^T$ in (4) of feedforward linearization reference control law of the 12th satellite.
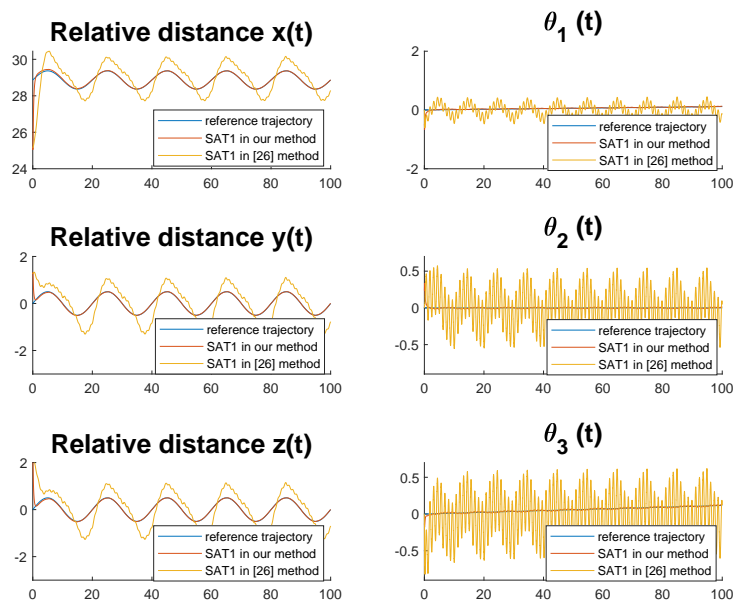
Figure 19. The attitude and altitude formation tracking performance of the 1st satellites with fault signals by the proposed decentralized H_∞ attack-tolerant observer-based PID team formation method in comparison with the decentralized H_∞ T-S fuzzy state feedback control method in [24].

four different orbits is given for a task of coverage service to validate a better team formation tracking performance of the proposed method in comparison with the H_∞ T-S fuzzy state feedback control method [24]. In future work, we will focus on event-trigger design for reserving network resources of the large-scale LEO satellite NCS.
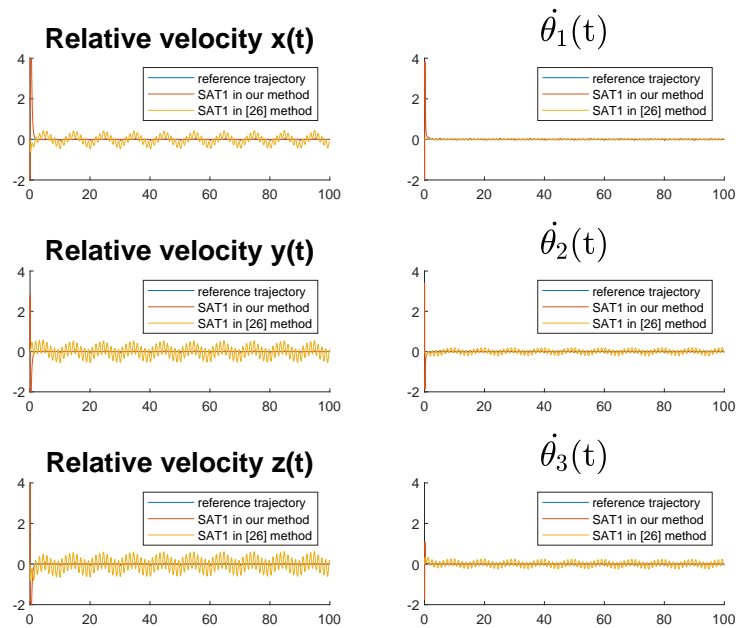
Figure 20. The relative velocity and angular velocity tracking performance of the 1st satellites with fault signals by the proposed method in comparison with the T-S fuzzy state feedback control method in [24]

Authors' contributions

Concept development and data acquisition: Chen, B. S.

Manuscript drafting: Liang, C. C.

Manuscript modification: Wang, L. H.

Availability of data and materials

All data and materials used in the research were produced by the authors as part of the study and explicitly detailed in the manuscript's methodology section.

Financial support and sponsorship

None.

Conflicts of interest

All authors declared that there are no conflicts of interest.

Ethical approval and consent to participate

Not applicable.

Consent for publication

Not applicable.

Copyright

NOMENCLATURE

$diag(X_1, X_2, \ldots, X_n)$	=	a block diagonal matrix with main diagonal blocks $X_1, X_2, \ldots, X_n$
A^T	=	the transpose of A
O	=	zero matrix
(a_n)	=	a sequence
(a_{k_n})	=	a subsequence of a sequence (a_n)

$[a_{j,k}]$	=	a matrix with the entries $a_{j,k}$ in the jth row and kth column
$|Z|$	=	size of a set Z
$\otimes$	=	Kronecker product
I_n	=	n-dimension identity matrix
$\begin{bmatrix} A & S \\ * & B \end{bmatrix}$	=	the symmetric matrix $\begin{bmatrix} A & S \\ S^T & B \end{bmatrix}$
$x(t) \in L_2[0, t_f]$	=	$\int_0^{t_f} x^T(t)x(t)dt < \infty$

REFERENCES

1. Leyva-Mayorga I, Soret B, Röper M, Wübben D, Matthiesen B, Dekorsy M. LEO small-satellite constellations for 5G and beyond-5G communications. *IEEE Access* 2020;8:184955-64. DOI

2. Srivastava R, Sah R, Das K. Attitude determination and control system for a leo debris chaser small satellite. San Diego, CA: AIAA SCITECH; 2022. p. 0519. DOI

3. Reid TGR, Chan B, Goel A, Gunning K, Manning B, Martin J. Satellite navigation for the age of autonomy. In Proceedings of the 2020 IEEE/ION Position, Location and Navigation Symposium (PLANS); 20-23 April 2020; Portland, OR, USA. pp. 342-52. DOI

4. Chaudhry AU, Yanikomeroglu H. Laser intersatellite links in a starlink constellation: a classification and analysis. *IEEE Veh Technol Mag* 2021;16:48-56. DOI

5. Scharf DP, Hadaegh FY, Ploen SR. A survey of spacecraft formation flying guidance and control (part 1): guidance. In Proceedings of the 2003 American Control Conference; 4-6 June 2003; Denver, CO, USA. pp. 1733-39. DOI

6. Du H, Chen MZQ, Wen G. Leader–following attitude consensus for spacecraft formation with rigid and flexible spacecraft. *J Guid Control Dynam* 2016;39:944-51. DOI

7. Wang PKC, Hadaegh FY. Minimum-fuel formation reconfiguration of multiple free-flying spacecraft. *J Astronaut Sci* 1999;47:77-102. DOI

8. Essghaier A, Beji L, El Kamel MA, Abichou A, Lerbet J. Co-leaders and a flexible virtual structure based formation motion control. *Int J Veh Auton Syst* 2011;9:108-25. DOI

9. Guo S, Pan Y, Li H, Cao L. Dynamic event-driven ADP for N-player nonzero-sum games of constrained nonlinear systems. *IEEE Trans Autom Sci Eng* 2024;1-13. DOI

10. Huang Y, Jia Y. Adaptive finite-time 6-DOF tracking control for spacecraft fly around with input saturation and state constraints. *IEEE Trans Aerosp Electron Syst* 2019;55:3259-72. DOI

11. Beard RW, Lawton J, Hadaegh FY. A coordination architecture for spacecraft formation control. *IEEE Trans Control Syst Technol* 2001;9:777-90. DOI

12. Pola G, Pepe P, Di Benedetto MD. Decentralized supervisory control of networks of nonlinear control systems. *IEEE Trans Autom Control* 2017;63:2803-17. DOI

13. Low CB. Adaptable virtual structure formation tracking control design for nonholonomic tracked mobile robots, with experiments. In Proceedings of the 2015 IEEE 18th International Conference on Intelligent Transportation Systems; 15-18 September 2015; Gran Canaria, Spain. pp. 1868-75. DOI

14. Yang A, Naeem W, Irwin GW, Li K. Stability analysis and implementation of a decentralized formation control strategy for unmanned vehicles. *IEEE Trans Control Syst Technol* 2013;22:706-20. DOI

15. Chang YH, Chang CW, Chen CL, Tao CW. Fuzzy sliding-mode formation control for multirobot systems: design and implementation. *IEEE Trans Syst Man Cyber Part B* 2011;42:444-57. DOI

16. Liu X, Ge SS, Goh CH, Li Y. Event-triggered coordination for formation tracking control in constrained space with limited communication. *IEEE Trans Cyber* 2018;49:1000-11. DOI

17. Liu X, Kumar KD. Network-based tracking control of spacecraft formation flying with communication delays. *IEEE Trans Aerosp Electron Syst* 2012;48:2302-14. DOI

18. Shui A, Chen W, Zhang P, Hu S, Huang X. Review of fault diagnosis in control systems. In Proceedings of the 2009 Chinese Control and Decision Conference; 17-19 June 2009; Guilin, China. pp. 5324-29. DOI

19. Harshavarthini S, Sakthivel R, Ahn CK. Finite-time reliable attitude tracking control design for nonlinear quadrotor model with actuator faults. *Nonlinear Dyn* 2019;96:2681-92. DOI

20. Saha RK. Spectrum sharing in satellite-mobile multisystem using 3D in-building small cells for high spectral and energy efficiencies in 5G and beyond era. *IEEE Access* 2019;7:43846-68. DOI

21. Zhang Z, Shi Y, Zhang Z, Zhang H, Bi S. Modified order-reduction method for distributed control of multi-spacecraft networks with time-varying delays. *IEEE Trans Control Netw Syst* 2016;5:79-92. DOI

22. Razzaghi P, Assadian N. Study of the triple-mass tethered satellite system under aerodynamic drag and J_2 perturbations. *Adv Space Res* 2015;56:2141-50. DOI

23. Vijayan R, Bilal M, Schilling K. Nonlinear dynamic modeling of satellite relative motion with differential J_2 and drag. In Proceedings of the 2020 IEEE Aerospace Conference; 7-14 March 2020; Big Sky, MT, USA. pp. 1-8. DOI

24. Chen BS, Ma YS, Lee MY. Stochastic robust H_∞ decentralized network formation tracking control of large-scale team satellites via event-triggered mechanism. *IEEE Access* 2022;10:62011-36. DOI

25. Chen BS, Lin HY. Decentralized H_∞ observer-based attack-tolerant formation tracking network control of large-scale LEO satellites via HJIE-reinforced deep learning approach. *IEEE Access* 2023;11:17165-96. DOI

26. Chen W, Hu Q, Guo L. Relative position fixed-time tracking control of spacecraft. In Proceedings of the 2017 36th Chinese Control Conference (CCC); 26-28 July 2017; Dalian, China. pp. 9466-71. DOI

27. Feng G. A survey on analysis and design of model-based fuzzy control systems. *IEEE Trans Fuzzy Syst* 2006;14:676-97. DOI

28. Amoozgar MH, Chamseddine A, Zhang Y. Fault-tolerant fuzzy gain-scheduled PID for a quadrotor helicopter testbed in the presence of actuator faults. *IFAC Proc Vol* 2012;45:282-7. DOI

29. Goodarzi F, Lee D, Lee T. Geometric nonlinear PID control of a quadrotor UAV on SE(3). In Proceedings of the 2013 European control conference (ECC); 17-19 July 2013; Zurich, Switzerland. pp. 3845-50. DOI

30. Alaimo A, Artale V, Milazzo CLR, Ricciardello A. PID controller applied to hexacopter flight. *J Intell Robot Syst* 2014;73:261-70. DOI

31. Kada B, Ghazzawi Y. Robust PID controller design for an UAV flight control system. In Proceedings of the World Congress on Engineering and Computer Science; 19-21 October 2011; San Francisco, USA. pp. 1-6. Available from: https://www.iaeng.org/publication/WCECS2011/WCECS2011_pp945-950.pdf [Last accessed on 31 Dec 2024]

32. Moreno-Valenzuela J, Pérez-Alcocer R, Guerrero-Medina M, Dzul A. Nonlinear PID-type controller for quadrotor trajectory tracking. *IEEE/ASME Trans Mech* 2018;23:2436-47. DOI

33. Nishiyama T, Suzuki S, Sato M, Masui K. Simple adaptive control with PID for MIMO fault tolerant flight control design. San Diego, CA: AIAA Infotech@Aerospace; 2016. p. 0132. DOI

34. Gonzalez H, Arizmendi C, Garcia J, Anguo A, Herrera C. Design and experimental validation of adaptive fuzzy PID controller for a three degrees of freedom helicopter. In Proceedings of the 2018 IEEE International Conference On Fuzzy Systems (FUZZ-IEEE); 8-13 July 2018; Rio de Janeiro, Brazil. pp. 1-6. DOI

35. Wang D, Wu B, Poh EK. Satellite formation flying: relative dynamics, formation design, fuel optimal maneuvers and formation maintenance. Springer; 2017. Available from: https://link.springer.com/book/10.1007/978-981-10-2383-5 [Last accessed on 31 Dec 2024]

36. Bahrami S, Namvar M. Rigid body attitude control with delayed attitude measurement. *IEEE Trans Control Syst Technol* 2015;23:1961-9. DOI

37. Varga RS. Extrapolation methods: theory and practice. *Numer Algor* 1993;3:305. DOI

38. Boyd S, El Ghaoui L, Feron E, Balakrishnan V. Linear matrix inequalities in system and control theory. Philadelphia, PA: SIAM; 1994. DOI

39. VanAntwerp JG, Braatz RD. A tutorial on linear and bilinear matrix inequalities. *J Proc Control* 2000;10:363-85. DOI

40. Yang L, Hasna MO. Performance analysis of amplify-and-forward hybrid satellite-terrestrial networks with cochannel interference. *IEEE Trans Commun* 2015;63:5052-61. DOI

41. Ishijima Y, Inaba N, Matsumoto A, Terada K, Yonechi H, Ebisutani H. Design and development of the first Quasi-Zenith Satellite attitude and orbit control system. In Proceedings of the 2009 IEEE Aerospace Conference; 7-14 March 2009; Big Sky, MT, USA. pp. 1-8. DOI